CHAPTER 3

VARIATIONAL METHOD FOR ANALYZING SEISMIC STABILITY OF VARIAOUS SOIL SLOPES

3.1 INTRODUCTION AND REVIEW OF EXISTING STUDIES

Almost for the last eight decades, the slope stability problems were studied rigorously by several researchers with the help of conventional limit equilibrium method. With the significant advancements in computational capabilities in recent decades, different numerical methods have been employed for slope stability analysis. Newmark (1965) developed the sliding block theory for estimating the permanent displacement of slopes during earthquakes. He considered the plane sliding surface for homogeneous dams and embankments consisting of cohesionless soil. Goodman and Seed (1966) proposed a planar rupture surface for earthquake-induced slope stability. They assumed the soil to be cohesionless. Sarma (1975) considered a circular rupture surface for homogeneous dams and embankments under seismic forces. Leshchinsky and San (1994) used Baker and Garber's (1978) variational approach to analyze the stability of slopes under seismic loading conditions with applied horizontal seismic acceleration. Ling and Leshchinsky (1995) predicted the seismic performances of slopes by considering a log-spiral failure surface. Kramer and Smith (1997) considered the dynamic response of soil above the slip surface and introduced the permanent displacement effect of soil above the rupture surface. Sarma (1999) calculated the seismic bearing capacity of shallow foundations constructed near sloping surfaces. Rathje and Bray (2000) analyzed the earth structure by considering nonlinear coupled seismic sliding. Wartman et al. (2003) studied the dynamic response and deformation

of rigid inclined blocks due to shaking using analytical methods. Choudhury et al. (2007) analyzed the stability of slopes under static and seismic conditions using the limit equilibrium approach. They considered the failure surface of the slope to be circular.

Several studies were also conducted to assess the undrained stability of nonhomogeneous clayey slopes, utilizing various methods such as (i) the limit equilibrium method (Gibson and Morgenstern 1962; Hunter and Schuster 1968; Koppula 1984a, 1984b; Low 1989), (ii) the upper bound rigid block method (Booker and Davis 1972 and Chen et al. 1975), (iii) the conventional displacement-based finite element method (Chai et al. 2009; Griffiths and Yu 2015), (iv) the finite element limit analysis method (Li et al. 2009, 2010), and (v) the variational method (Li et al. 2018). Investigations on stability were also performed for soil slopes comprising of different combinations of soil layers (Loukidis et al. 2003; Zolfaghari et al. 2005; Kumar and Samui 2006; Hammouri et al. 2008; Kahatadeniya et al. 2009; Shiau et al. 2011; Li et al. 2012; Qian et al. 2014; Lim et al. 2015; Qin and Chain 2017; Deng et al. 2019; Li et al. 2020; Zuo et al. 2022). Loukidis et al. (2003) employed limit analysis to examine the stability of a three-layered soil slope under seismic loading conditions. Zolfaghari et al. (2005) analyzed the stability of layered soil slopes under the influence of vertical and horizontal seismic forces, as well as surcharge loads, using a genetic algorithm to consider non-circular slip surfaces. Kumar and Samui (2006) computed the stability of layered soil slopes subjected to pore-water pressure and horizontal seismic force through upper bound limit analysis. Hammouri et al. (2008) assessed the stability analysis of the layered slopes by considering the effects of rapid drawdown and tension cracks with the aid of PLAXIS 8.0 and SAS-MCT 4.0 software. Kahatadeniya et al. (2009) used ant colony optimization to identify the critical failure plane of layered soil

slopes that were exposed to vertical and horizontal pseudo-static forces, as well as uniform vertical overburden forces. Shiau et al. (2011) and Qian et al. (2014) examined the undrained stability of two-layered purely cohesive soil slopes by applying the finite element limit analysis. Li et al. (2012) investigated the stability of a layered slope that experiences both vertical and horizontal pseudo-static forces by identifying the sliding surface. On the other hand, Qin and Chain (2017) analyzed the stability of a two-stage layered slope that contains a strip footing located close to the top of the slope under the influence of pseudo-static vertical and horizontal forces. By employing the finite element LB limit analysis method, Lim et al. (2015) provided stability charts for frictional fill material placed on purely cohesive soil. Deng et al. (2019) developed a limit-equilibrium stress method and established a failure mechanism for analyzing the stability of layered slopes using composite slip surfaces. Li et al. (2020) analysed three layered soil slopes by considering an artificial neural network (ANN) and finite element limit analysis technique. On the basis of upper bound limit analysis, Zuo et al. (2022) extended the log-spiral rotational failure mechanism for layered slopes using a multicentre method.

From the available literature, it can be concluded that very few research works on homogeneous and heterogeneous soil slopes under seismic forces by using the variational approach had been carried out earlier. This was the prime motive behind the work presented in the current chapter. By using variational approach, it is intended to determine the critical factor of safety and corresponding failure surface of four types of soil slopes, namely (i) homogeneous cohesive-frictional slope, (ii) heterogeneous (continuously varying cohesion) slopes, (iii) two-layered cohesive-frictional slope, (iv) two-layered slopes where cohesive-frictional soil is placed over non-homogenous cohesive soil. The Mohr-Coulomb (MC) criterion is chosen to model the saturated soil

conditions. The computed results obtained from the analysis have been compared with the available solutions in the literature.

3.2 PROBLEM STATEMENT

A rectilinear slope of angle, β, is subjected to certain seismic loadings. Based on the soil configurations, the following four cases are considered:

Case 1: Homogeneous c-ϕ soil

Case 2: Non-homogeneous undrained cohesive soil (ϕ_u=0°)

Case 3: Two layered cohesive-frictional soil

Case 4: Homogeneous c-ϕ soil underlain by non-homogeneous clays

Fig. 3.1 shows the considered cases along with the chosen domain. The heterogeneity of the clay layer in Cases 2 and 4 are realized by the following linear relationship, as proposed by Bishop (1961) for normally-consolidated, undrained, and completely saturated clays:

$$c_u = c_{u0} + mz \tag{3.1}$$

This equation shows the linear increment of cohesion (c_u) with depth. Here, (i) m indicates the gradient at which the undrained shear strength increases, and (ii) c_{u0} and c_u are the undrained shear strength of clays at the top surface of the cohesive layer and at a certain depth, z, below the ground surface, respectively. The top surface of the cohesive layer is the ground surface (for Case 2) or the layered interface (for Case 4). For Case 3, the strength parameters of the top and bottom layers are (c_1, ϕ_1) and (c_2, ϕ_2), respectively.

Based on the past few studies, the analysis procedure is simplified by idealizing the inertial forces in the dynamic loading with the pseudo-static forces. According to D'alembert's principle, the pseudo-static forces are computed by using the product of

mass and acceleration. Despite its inherent limitations, the pseudo-static method is simple, inexpensive, less time-consuming, and provides reasonably satisfactory solutions for many practical scenarios.

For all four cases, the soil is considered isotropic and governed by Mohr-Coulomb (MC) failure criterion. The size of the domain is kept adequately large enough so that the failure or slip surface remains within the domain, and it is noted that the domain size does not influence the computed solution. It is intended to determine the critical failure surface and corresponding critical factor of safety (F_s) for the considered four slopes.

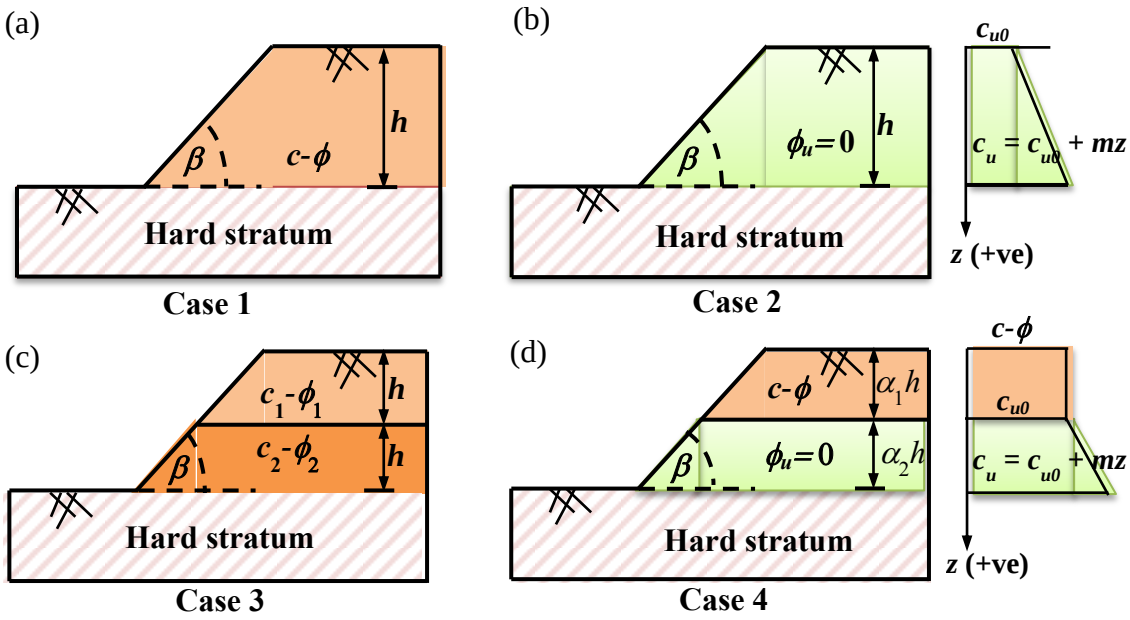

Fig 3.1 Schematic diagram of considered slopes for (a) Case 1, (b) Case 2, (c) Case 3, and (d) Case 4.

3.3 ANALYSIS PROCEDURE

To analyze the stability of a slope, the variational method is employed within the framework of the ordinary method of slice, as proposed by Fellenius (1936).

Broadly speaking, obeying Revilla and Castillo (1977) and Baker and Garber (1978), the following steps are employed for finding the critical factor of safety:

Step 1: Obtaining the discrete formulation of factor of safety (F)

Step 2: Transforming the discrete formulation into an integral form

Step 3: Identifying the functional forms

Step 4: Employing the Euler-Lagrangian equation to obtain the expression of F_s

Step 5: Integrating (twice) the expression of F_s to obtain the form of slip surfaces

Step 6: Evaluating the unknown parameters of Step 5 by enforcing the following criteria: (a) transversality, (b) continuity, (c) natural boundary, and (d) intersection conditions

3.3.1 Step 1: Obtaining the discrete formulation of *F*

The soil encompassed within an arbitrary slip surface is discretized into n segments (as shown in Fig. 3.2a). The resisting shear strength and the mobilized shear stress developed along the entire slip surface is considered to be the summation of the corresponding components along each slice. The free-body diagram of an arbitrary slice is demonstrated in Fig. 3.2b. The discrete formulation of F is obtained by using the conventional definition of factor of safety along with the Mohr-Coulomb yield equation in $\tau - \sigma_n$ space and the force equilibrium equations. Mathematically, F is written as:

$$F = \frac{\text{available shear strength}}{\text{mobilized shear stress}} = \frac{\sum_{i=1}^{n} \tau_f}{\sum_{i=1}^{n} \tau_i} = \frac{\sum_{i=1}^{n} \left[c + \sigma_{ni} \tan \varphi \right]}{\sum_{i=1}^{n} \tau_i} \qquad (3.2)$$

Here, σ_{ni} and τ_i are the normal and shear stresses developed in an arbitrary i^{th} slice.

The expressions of σ_{ni} and τ_i are obtained by satisfying the static equilibrium equations for the slice, *i*, along *x* and *y* directions:

$$\sigma_{ni} = \frac{N_i}{\Delta l_i} = \frac{(W_i - F_{vi})\cos\theta_i - F_{hi}\sin\theta_i}{\Delta l_i} \tag{3.3a}$$

$$\tau_i = \frac{S_i}{\Delta l_i} = \frac{W_i \sin\theta_i + F_{hi}\cos\theta_i - F_{vi}\sin\theta_i}{\Delta l_i} \tag{3.3b}$$

where, (i) Δx_i, θ_i, and Δl_i ($=\Delta x_i/\cos\theta_i$) are the width, inclination angle and the length of the i^{th} slice (as shown in Fig. 3.2), respectively; (ii) W_i represents weight and F_{vi} ($=k_v W_i$) and F_{hi} ($=k_h W_i$) are the vertical and horizontal pseudo-static forces acting on the i^{th} slice, and (iii) *n* represents the total number of slices. Here, k_h and k_v are the horizontal and vertical seismic acceleration coefficients, respectively.

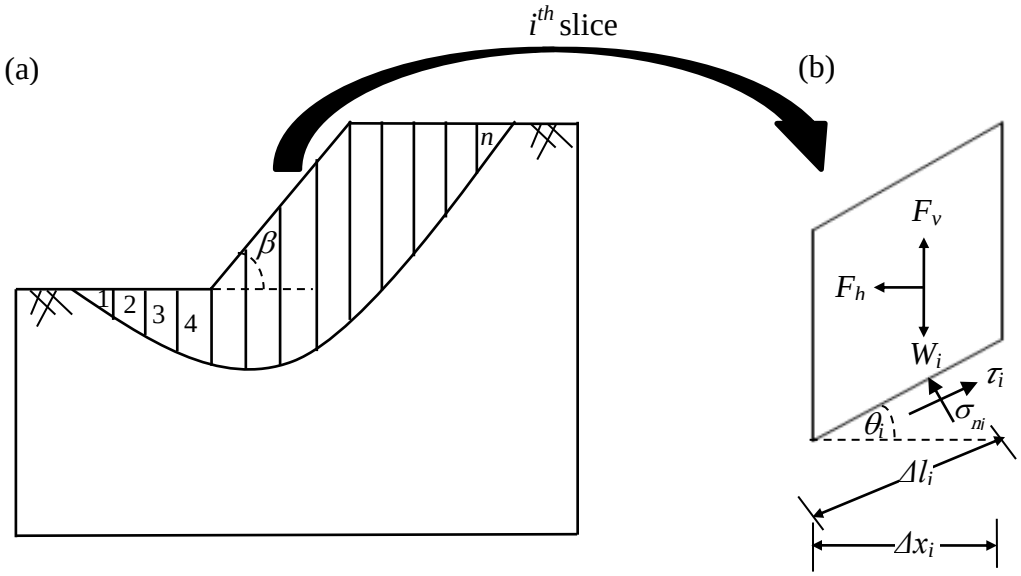

Fig 3.2 (a) Arbitrary slip surface with *n* number of discretized segments, (b) force distribution in any arbitrary i^{th} slice.

Substituting Eq. (3.3a) and Eq. (3.3b) into Eq. (3.2), and plugging the expressions of F_v, F_h and Δl_i, the following expressions of factor of safety are obtained.

Case 1 and 3:
$$F = \frac{\sum_{i=1}^{n}\left[c\Delta x_i \sec^2\theta_i + W_i\{(1-k_v) - k_h \tan\theta_i\}\tan\phi\right]}{\sum_{i=1}^{n} W_i\left[(1-k_v)\tan\theta_i + k_h\right]} \quad (3.4)$$

Case 2:
$$F = \frac{\sum_{i=1}^{n}\left[c_u \Delta x_i \sec^2\theta_i\right]}{\sum_{i=1}^{n} W_i\left[(1-k_v)\tan\theta_i + k_h\right]} \quad (3.5)$$

Case 4:
$$F = \frac{\sum_{i=1}^{n}\left[(c_{u0} + mz)\Delta x_i \sec^2\theta_i + W_i\{(1-k_v) - k_h \tan\theta_i\}\tan\phi\right]}{\sum_{i=1}^{n} W_i\left[(1-k_v)\tan\theta_i + k_h\right]} \quad (3.6)$$

3.3.2 Step 2: Transforming the discrete formulations into integral forms

The discrete formulations (as demonstrated in Eq. 3.4-3.6) are being transformed into the continuous form by considering the width of the slice to be very small ($\Delta x_i \to 0$). Table 3.1 shows the integral form of F. In this expression, the weight of each slice is expressed as: $W_i = \gamma(f_i - y_i)\Delta x_i$; where, γ is the unit weight of soil, and f_i and y_i represent the slope and the slip surfaces, respectively. The slope surface is defined distinctly in each region marked in the defined domain. Fig. 3.3 shows the demarcation of the regions. The domain corresponding to Cases 1 and 2 and Cases 3 and 4 are divided in three and four regions, respectively. Table 3.2 shows the expression of the slope surfaces in each region. The expression of the slip surface for a certain region will be unique owing to the fact that the form of the slope surface within each region is constant. Hence, the complete form of the slip surface can be found by distinctively computing the equation of $y_i(x)$ in each region.

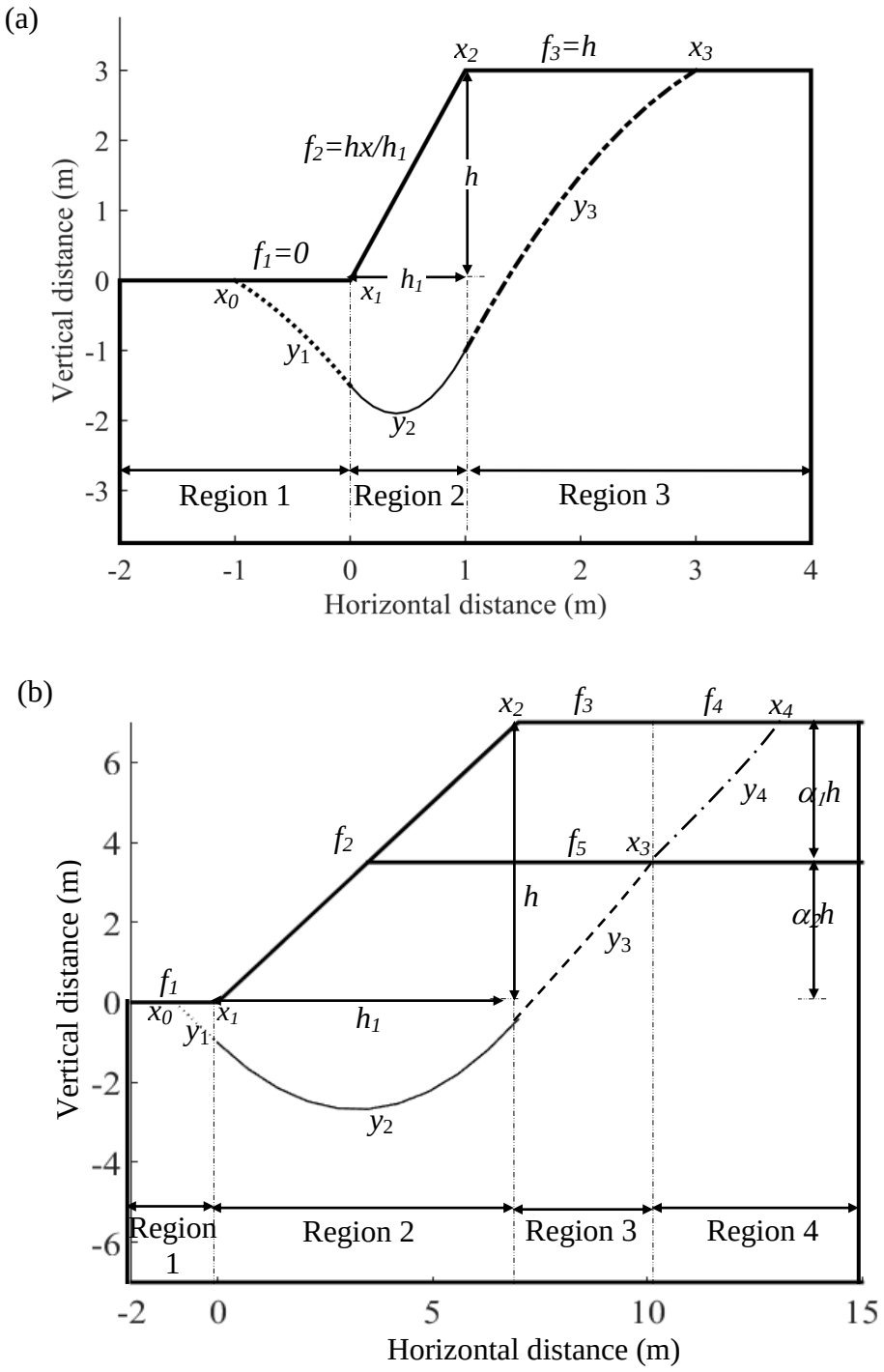

Fig. 3.3 Form of the failure slip surface computed by variational method for (a) Case 1, 2 and (b) Case 3, 4.

Table 3.1 The integral expressions of for the corresponding cases

Cases	Integral expressions of F
Case1 and 3	$F = \lim_{\Delta x_i \to 0} \frac{\sum_{i=1}^{n}\left[c\Delta x_i \sec^2\theta_i + W_i\{(1-k_v)-k_h\tan\theta_i\}\tan\phi\right]}{\sum_{i=1}^{n} W_i\left[(1-k_v)\tan\theta_i + k_h\right]} = \frac{\int_{x_0}^{x_n}\left[c\left(1+y_i'^2\right)+\gamma(f_i-y_i)\{(1-k_v)-k_h y_i'\}\tan\phi\right]dx}{\int_{x_0}^{x_n}\gamma(f_i-y_i)\left[(1-k_v)y_i'+k_h\right]dx}$
Case 2	$F = \lim_{\Delta x_i \to 0} \frac{\sum_{i=1}^{n}\left[c_u\Delta x_i \sec^2\theta_i\right]}{\sum_{i=1}^{n} W_i\left[(1-k_v)\tan\theta_i + k_h\right]} = \frac{\int_{x_0}^{x_n}\left[c_u\left(1+y_i'^2\right)\right]dx}{\int_{x_0}^{x_n}\gamma(f_i-y_i)\left[(1-k_v)y_i'+k_h\right]dx}$
Case 4	$F = \lim_{\Delta x_i \to 0} \frac{\sum_{i=1}^{n}\left[(c_{u0}+mz)\Delta x_i \sec^2\theta_i + W_i\{(1-k_v)-k_h\tan\theta_i\}\tan\phi\right]}{\sum_{i=1}^{n} W_i\left[(1-k_v)\tan\theta_i + k_h\right]} = \frac{\int_{x_0}^{x_n}\left[(c_{u0}+mz)\left(1+y_i'^2\right)+\gamma(f_i-y_i)\{(1-k_v)-k_h y_i'\}\tan\phi\right]dx}{\int_{x_0}^{x_n}\gamma(f_i-y_i)\left[(1-k_v)y_i'+k_h\right]dx}$

Note: (i) $y_i' = \tan\theta_i$, (ii) $W_i = \gamma(f_i - y_i)\Delta x_i$; and, (iii) x_0 and x_n are the endpoints' abscissas where the slip surface intersect with the slope surface.

Table 3.2 The expression of the slope surfaces in the divided regions

Cases	Region 1 $x_0 \le x \le x_1$ (= 0)	Region 2 $x_1 < x < x_2$ (= h_1)	Region 3 $x_2 \le x \le x_3$	Region 4 $x_3 \le x \le x_4$
Case 1 and 2	$f_1(x) = 0$	$f_2(x) = \frac{h}{h_1}x$	$f_3(x) = h$	––
Case 3 and 4	$f_1(x) = 0$	$f_2(x) = \frac{h}{h_1}x$	$f_3(x) = h$	$f_4(x) = h$

3.3.3 Step 3: Identifying the functional forms

From Table 3.1, it is well observed that the denominator and the numerator of F explicitly depend on the x-coordinates, slip and slope surfaces. The slip (y) and the slope (f) surfaces are unknown and known functions of x-coordinates, respectively. Therefore, the factor of safety can be represented as a ratio of two functionals which can be expressed as follows:

$$F = \frac{\int_{x_0}^{x_n} P_i(x, y, y')dx}{\int_{x_0}^{x_n} R_i(x, y, y')dx} \tag{3.7}$$

Table 3.3 depicts the expressions of P_i and R_i functionals for all the four cases. The integral expression can be further divided in the chosen regions.

Table 3.3 The expression of P_i and R_i for four cases

Cases	P_i		R_i
Case1	$\left[c\left(1+y_i'^2\right)+\gamma\left(f_i-y_i\right)\times\left\{\left(1-k_v\right)-k_h y_i'\right\}\tan\phi\right]$	$i=1, 2, 3$	$\gamma\left(f_i-y_i\right)\times\left\{\left(1-k_v\right)y_i'+k_h\right\}$
Case2	$\left[c_u\left(1+y_i'^2\right)\right]$		
Case3	$\left[c\left(1+y_i'^2\right)+\gamma\left(f_i-y_i\right)\times\left\{\left(1-k_v\right)-k_h y_i'\right\}\tan\phi\right]$	$i=1, 2, 3, 4$	
Case4	$\left[\left(c_{u0}+mz\right)\left(1+y_i'^2\right)+\gamma\left(f_i-y_i\right)\times\left\{\left(1-k_v\right)-k_h y_i'\right\}\tan\phi\right]$		

The expression of the factor of safety in Eq. (3.7) takes the following form (x_i coordinates are marked in Fig. 3.3a and 3.3b):

Case 1, 2:
$$F = \frac{\int_{x_0}^{x_1} P_1(x,y,y')dx + \int_{x_1}^{x_2} P_2(x,y,y')dx + \int_{x_2}^{x_3} P_3(x,y,y')dx}{\int_{x_0}^{x_1} R_1(x,y,y')dx + \int_{x_1}^{x_2} R_2(x,y,y')dx + \int_{x_2}^{x_3} R_3(x,y,y')dx} \tag{3.8}$$

Case 3, 4: $$F=\frac{\int_{x_0}^{x_1}P_1(x,y,y')dx+\int_{x_1}^{x_2}P_2(x,y,y')dx+\int_{x_2}^{x_3}P_3(x,y,y')dx+\int_{x_3}^{x_4}P_4(x,y,y')dx}{\int_{x_0}^{x_1}R_1(x,y,y')dx+\int_{x_1}^{x_2}R_2(x,y,y')dx+\int_{x_2}^{x_3}R_3(x,y,y')dx+\int_{x_3}^{x_4}R_4(x,y,y')dx} \quad (3.9)$$

3.3.4 Step 4: Employing the Euler-Lagrangian equation to obtain the expression of F_s

To obtain the critical slip surface, which corresponds to the critical factor of safety (F_s), the above functionals (F) must be minimized using the Euler-Lagrangian equation as follows:

$$F_s=\frac{\frac{\partial P}{\partial y_i}-\frac{d}{dx}\left(\frac{\partial P}{\partial y_i'}\right)}{\frac{\partial R}{\partial y_i}-\frac{d}{dx}\left(\frac{\partial R}{\partial y_i'}\right)} \quad (3.10)$$

By employing Euler-Lagrangian equation the expression of critical factor of safety for four cases can be depicted as follows:

Case 1: $$F_S=\frac{2cy_i''+\gamma\tan\phi\left[(1-k_v)-f_i'k_h\right]}{\gamma\left[(1-k_v)f_i'+k_h\right]};\qquad (i=1,2,3) \quad (3.11)$$

Case 2: $$F_S=\frac{2c_u y_i''}{\gamma\left[(1-k_v)f_i'+k_h\right]};\qquad (i=1,2,3) \quad (3.12)$$

Case 3: $$F_S=\frac{2cy_i''+\gamma\tan\phi\left[(1-k_v)-f_i'k_h\right]}{\gamma\left[(1-k_v)f_i'+k_h\right]};\qquad (i=1,2,3,4) \quad (3.13)$$

Case 4: $$F_S=\frac{2(c_{u0}+mz)y_i''+\gamma\tan\phi\left[(1-k_v)-f_i'k_h\right]}{\gamma\left[(1-k_v)f_i'+k_h\right]};\quad (i=1,2,3,4) \quad (3.14)$$

3.3.5 Step 5: Integrating (twice) the expression of F_s to obtain the form of slip surfaces

Corresponding to each case, the slip surfaces in the prescribed regions can be obtained by integrating Eqs. (3.11-3.14) twice. These surfaces are constructed by assuming that the factor of safety remains constant along the entire slip surface. After performing the integration, the generalized quadratic form of the slip surface in each region can be expressed as below:

$$y_i = A_i x^2 + B_i x + D_i \text{;} \quad \text{(Case 1, 2: } i\text{=1, 2, 3; Case 3, 4: } i\text{=1, 2, 3, 4)} \quad (3.15)$$

Here, (a) A_i's are the known coefficients presented in Table 3.4

(b) B_i's and D_i's are the unknown integration constants.

Table 3.4 The expression of A_i for four cases.

Case 1	Case 2
$A_1 = A_3 = -\frac{\gamma}{4c}\tan\phi(1-k_v) + \frac{k_h}{4Nh}$ $A_2 = -\frac{\gamma}{4c}\tan\phi\left\{(1-k_v) - \frac{h}{h_1}k_h\right\}$ $+ \frac{1}{4Nh}\left\{(1-k_v)\frac{h}{h_1} + k_h\right\}$ Here, $N(=c/F_S\gamma h)$ indicates the stability number.	$A_1 = A_3 = \frac{k_h}{4(1+\lambda)Nh}$; $A_2 = \frac{\left[(1-k_v)\frac{h}{h_1} + k_h\right]}{4(1+\lambda)Nh}$ Here, N ($=c_{u0}/(F_s\gamma h)$) and λ($=mh/c_{u0}$) indicate the stability number and the cohesion coefficient, respectively.
Case 3	**Case 4**
$A_1 = A_3 = -\frac{\gamma}{4c_2}\tan\phi_2(1-k_v) + \frac{\alpha k_h}{8Nh}$ $A_2 = -\frac{\gamma}{4c_2}\tan\phi_2\left\{(1-k_v) - \frac{2h}{h_1}k_h\right\}$ $+ \frac{\alpha}{8Nh}\left\{(1-k_v)\frac{2h}{h_1} + k_h\right\}$ $A_4 = -\frac{\gamma}{4c_1}\tan\phi_2(1-k_v) + \frac{k_h}{8Nh}$ Here, N ($=c_1/(2F_s\gamma h)$) indicates the stability number. α ($=c_1/c_2$) represents the ratio of cohesion of two layers.	$A_1 = A_3 = \frac{k_h}{4(1+\lambda)Nh}$; $A_2 = \frac{\left[(1-k_v)\frac{h}{h_1} + k_h\right]}{4(1+\lambda)Nh}$ $A_4 = -\frac{\gamma\tan\phi(1-k_v)}{4c_{u0}} + \frac{k_h}{4Nh}$ Here, λ($=m\alpha_2 h/c_{u0}$) and N ($=c_{u0}/(F_s\gamma h)$) indicate the cohesion coefficient and the stability number, respectively.

The equation of slip surface in each region consists of two unknown integration constants. Cases 1 and 2 involve three regions each, contributing to a total of six integration constants (3 B_i's and 3 D_i's). Additionally, as the shape of the failure surface remains unspecified, the endpoints (x_0 and x_3) and the critical factor of safety (F_s) are also unknown. In both Cases 3 and 4, featuring four regions each, the existence of eight unknown integration constants (4 B_i's and 4 D_i's) is noted. The uncertainty surrounding the shape of the failure surface encompasses the undetermined endpoints (x_0 and x_4), intersection point of the slip surface and the interface layer (x_3) and the critical factor of safety (F_s).

For Cases 1 and 2, there are total nine unknown parameters:

(i) x_0 and x_3 (two endpoints), (ii) F_s and (iii) 3 B_i's and 3 D_i's.

For Cases 3 and 4 total number of unknown parameters are twelve:

(i) x_0, x_4 (two end points), x_3 (intersection point of the slip surface and the interface layer), (ii) F_s and (iii) 4 B_i's and 4 D_i's.

The end points can also be regarded as the intersection points, denoting the locations where the slip surface and slope surface intersect each other.

3.3.6 Step 6: Evaluating the unknown parameters of Step 5

To obtain a well-defined, smoothened, continuous slip surface the following constraints are enforced:

(a) Two transversality conditions specified at two end-points of the boundary surfaces

$$[P_{y'}-F_S R_{y'}][f'(x)-y'(x)]+P-F_S R|_{x=x_i}=0;\ \begin{vmatrix} i=0,3 \text{ (For Cases 1 and 2)} \\ i=0,4 \text{ (For Cases 3 and 4)} \end{vmatrix} \quad (3.16)$$

(b) Continuity conditions specified at the intermediate points:

$$y_i(x_i) = y_{i+1}(x_i)\Big|_{i=1,2,3}^{i=1,2} \begin{matrix} \text{(For Cases 1 and 2)} \\ \text{(For Cases 3 and 4)} \end{matrix} \quad (3.17)$$

(c) Natural boundary conditions specified at the intermediate points

$$y_i'(x_i) = y_{i+1}'(x_i)\Big|_{i=1,2,3\ \text{(For Cases 3, 4)}}^{i=1,2\ \text{(For Cases 1, 2)}} \tag{3.18}$$

(d) Intersection conditions of slip and the slope surfaces:

Case 1 and 2: $y_1(x_0) = f_1(x_0);\ y_3(x_3) = f_3(x_3)$ (3.19)

Case 3 and 4: $y_1(x_0) = f_1(x_0);\ y_4(x_4) = f_4(x_4);\ y_3(x_3) = f_5(x_3)$ (3.20)

where, $f_5(x) = h\left(h_1 \le x \le x_3\right)$ (for Case 3);

$f_5(x) = \alpha_2 h\left(h_1 \le x \le x_3\right)$ (for Case 4); α_2=bottom layer thickness coefficient

(e) The equation for Factor of Safety, as provided in Eq. (3.8) for Cases 1 and 2 and in Eq. (3.9) for Cases 3 and 4.

3.3.6.1 Determining the integration constants and stability numbers

It appears that Cases 1 and 2 generate nine known equations and Cases 3 and 4 give rise to a total number of twelve known equations. As the number of equations and unknowns are the same, therefore the system guarantees to provide a unique solution. Table 3.5 shows the expression of the unknown integration constants and Table 3.6 shows the expression of the stability number (N) for all the considered cases.

3.3.6.2 Determining the intersection points

Most of the seismic failures in homogenous soil slopes are reported (Leshchinsky and San 1994; Ling et. al 1997; Ausilo et. al 2000; Loukidis et. al 2003) to fail by developing toe failure surface. A few literature (Griffiths and Yu 2015; Li et al. 2018) also reported that non-homogeneous soil slope under seismic condition fails by developing toe failure surface (x_0=0). Hence, in the present analysis, the value of x_0 is invariably considered equal to zero. However, the present formulations can be further extended for base and slope failures.

Table 3.5 The formulation of integration constants for four cases.

	B_i's	D_i's
Case1	$B_1 = B_2 = -1 + \frac{\gamma \tan\phi(1-k_v)}{2c} x_0 - \frac{k_h}{2Nh} x_0$ $B_3 = 1 + \frac{0.5\gamma \tan\phi(1-k_v)}{c} x_3 - \frac{0.5k_h}{Nh} x_3$	$D_1 = D_2 = x_0 - \frac{\gamma \tan\phi(1-k_v)}{4c} x_0^2 + \frac{k_h}{4Nh} x_0^2$ $D_3 = \frac{\gamma h h_1 k_h \tan\phi}{4c} + \frac{h_1(1-k_v)}{4N} + \frac{\gamma h_1 \tan\phi(1-k_v)(x_0 - x_3)}{2c} - \frac{k_h h_1 (x_0 - x_3)}{2Nh} + \frac{k_h x_0^2}{4Nh} - 2h_1 + x_0 - \frac{\gamma \tan\phi(1-k_v) x_0^2}{4c}$
Case2	$B_1 = B_2 = -1 - \frac{k_h x_0}{2(1+\lambda)Nh}; B_3 = 1 - \frac{0.5k_h x_3}{(1+\lambda)Nh}$	$D_1 = D_2 = x_0 + \frac{k_h x_0^2}{4(1+\lambda)Nh}$ $D_3 = \frac{(1-k_v)h_1}{4(1+\lambda)N} - 2h_1 + x_0 + \frac{k_h h_1 (x_3 - x_0)}{2(1+\lambda)Nh} + \frac{k_h x_0^2}{4(1+\lambda)Nh}$
Case3	$B_1 = B_2 = -1 + \frac{\gamma x_0}{2c_2} \tan\phi_2 (1-k_v) - \frac{\alpha k_h}{4Nh} x_0$ $B_3 = \frac{\gamma x_3}{2}(1-k_v)\left(\frac{\tan\phi_2}{c_2} - \frac{\tan\phi_1}{c_1}\right) + \frac{k_h x_3}{4Nh}(1-\alpha) + B_4$	$D_1 = D_2 = x_0 - \frac{\gamma x_0^2}{4c_2} \tan\phi_2 (1-k_v) + \frac{\alpha k_h x_0^2}{8Nh}; D_4 = \frac{\gamma x_3^2}{4}(1-k_v)\left(\frac{\tan\phi_2}{c_2} - \frac{\tan\phi_1}{c_1}\right) + \frac{k_h x_3^2}{8Nh}(1-\alpha) + D_3$ $D_3 = \frac{\gamma h h_1}{2c_2} \tan\phi_2 k_h + \frac{\alpha h_1 (1-k_v)}{4N} - 2h_1 + x_0 - \frac{\gamma h_1 \tan\phi_2 (1-k_v)(x_3 - x_0)}{2c_2} - \frac{\gamma h_1 \tan\phi_1 (1-k_v)(x_4 - x_3)}{2c_1} + \frac{\alpha h_1 k_h (x_3 - x_0)}{4Nh} + \frac{h_1 k_h (x_4 - x_3)}{4Nh} - \frac{\gamma x_0^2 \tan\phi_2 (1-k_v)}{4c_2} + \frac{\alpha k_h x_0^2}{8Nh}$
Case4	$B_1 = B_2 = -1 - \frac{0.5k_h x_0}{(1+\lambda)Nh}$ $B_3 = \left[\frac{k_h}{2Nh} - \frac{k_h}{2(1+\lambda)Nh} - \frac{\gamma \tan\phi(1-k_v)}{2c_{u0}}\right] x_3 + B_4$ $B_4 = 1 + \frac{\gamma \tan\phi(1-k_v)}{2c_{u0}} x_4 - \frac{k_h x_4}{2Nh}$	$D_1 = D_2 = x_0 + \frac{k_h x_0^2}{4(1+\lambda)Nh}$; $D_4 = \frac{k_h x_3^2}{4Nh} - \frac{k_h x_3^2}{4(1+\lambda)Nh} - \frac{\gamma \tan\phi(1-k_v)}{4c_{u0}} x_3^2 + D_3$ $D_3 = \frac{(1-k_v)h_1}{4(1+\lambda)N} - 2h_1 + x_0 - \frac{k_h x_0 h_1}{2(1+\lambda)Nh} + \frac{k_h x_0^2}{4(1+\lambda)Nh} - \left[\frac{k_h}{2Nh} - \frac{k_h}{2(1+\lambda)Nh} - \frac{\gamma \tan\phi(1-k_v)}{2c_{u0}}\right] x_3 h_1 - \left[\frac{\gamma \tan\phi(1-k_v)}{2c_{u0}} - \frac{k_h}{2Nh}\right] x_4 h_1$

For Cases 1 and 2, the closed-form expression of the other end point, x_3 is easily attainable. However, for Cases 3 and 4, the additional intersection point, x_3 generate nonlinear sets of algebraic equations which are implicit in nature; this prevents in achieving straight-forward analytical solution of the end point x_4.

Case 1:
$$x_3 = \frac{-B + \sqrt{B^2 - 4AC}}{2A} \tag{3.21}$$

where,
$$A = \frac{\gamma h \tan\phi (1-k_v)^2}{4c} + \frac{\gamma h \tan\phi k_h^2}{4c} \quad ; \quad C = -hh_1(1-k_v) - h^2(1-k_v)$$

$$B = h(1-k_v) - hk_h - \frac{\gamma h h_1 k_h^2 \tan\phi}{4c} - \frac{\gamma h h_1 \tan\phi (1-k_v)^2}{4c}$$

Case 2:
$$x_3 = \frac{(1-k_v)(h_1+h)}{[(1-k_v)-k_h]} \tag{3.22}$$

Case 3: The x_3 and x_4 are obtained by using Newton-Raphson method, as done for Case 4 too. The detailed description is there in Case 4.

Table 3.6 The expression of N for four cases.

Cases	Expression for N
Case 1	$N = \dfrac{(1-k_v) + \dfrac{k_h}{h}(x_3 - x_0)}{4 - \dfrac{\gamma h \tan\phi\, k_h}{c} + \dfrac{\gamma \tan\phi (1-k_v)(x_3 - x_0)}{c}}$
Case 2	$N = \dfrac{h(1-k_v) + k_h(x_3 - x_0)}{4(1+\lambda)h}$
Case 3	$N = \dfrac{\left[\alpha(1-k_v) + \dfrac{\alpha k_h}{2h}(x_3 - x_0) + \dfrac{k_h}{2h}(x_4 - x_3)\right]}{\left[4 - \dfrac{2\gamma h k_h \tan\phi_2}{c_2} + \dfrac{\gamma \tan\phi_2 (1-k_v)(x_3 - x_0)}{c_2} + \dfrac{\gamma \tan\phi_1 (1-k_v)(x_4 - x_3)}{c_1}\right]}$
Case 4	$N = \dfrac{[H(1-k_v) + k_h(x_3 - x_0) + k_h(1+\lambda)(x_4 - x_3)]}{H(1+\lambda)\left[4 + \dfrac{\gamma \tan\phi (1-k_v)}{c_{u0}}(x_4 - x_3)\right]}$

Case 4: Eq. (3.20) generates the following two nonlinear equations in terms of x_3 and x_4.

$$g_1(x_3, x_4): M_1 x_4^2 - M_2 x_3^2 + M_3 x_0^2 + M_4 x_3 h_1 - M_5 x_4 h_1 - M_6 x_0 + M_7 = 0 \quad (3.23)$$

$$g_2(x_3, x_4): -(2M_1 + M_3)x_3^2 + (1 + 2M_1 x_4)x_3 + M_3 x_0^2 + M_4 x_3 h_1 - M_5 x_4 h_1 - M_6 x_0 + M_8 = 0 \quad (3.24)$$

where, $M_1 = \dfrac{\gamma \tan\phi(1-k_v)}{4c_{u0}} - \dfrac{k_h}{4Nh}$; $\quad M_5 = 2M_1 + \dfrac{1}{h_1}$;

$M_2 = M_1 + \dfrac{k_h}{4(1+\lambda)Nh}$; $\quad M_6 = 2M_3 h_1 - 1$;

$M_3 = M_2 - M_1$; $\quad M_7 = \dfrac{(1-k_v)h_1}{4(1+\lambda)N} - 2h_1 - h$;

$M_4 = 2(M_1 + M_3)$; $\quad M_8 = \dfrac{(1-k_v)h_1}{4(1+\lambda)N} - 2h_1 - \alpha_2 h$

The system of equations can be represented in the compact form as: $g(X) = 0$ (3.25)

where, $g(X) = [g_1(X) \;\; g_2(X)]^T$, $X = [x_3 \;\; x_4]^T$ and $0 = [0 \;\; 0]^T$

The step-wise procedure for solving Eq. (3.25) is mentioned below:

Step 1: Start with initial guess of the unknown vector, X and set the initial counter k as

1.

Step 2: Compute the Jacobian (J) matrix @ k^{th} iteration using the following equation

$$J^{(k)} = \begin{bmatrix} \dfrac{\partial g_1(X^k)}{\partial x_3} & \dfrac{\partial g_1(X^k)}{\partial x_4} \\ \dfrac{\partial g_2(X^k)}{\partial x_3} & \dfrac{\partial g_2(X^k)}{\partial x_4} \end{bmatrix} \quad (3.26)$$

Step 3: Compute the unknown vector, X, at $(k+1)^{th}$ iteration as follows:

$$X^{(k+1)} = X^{(k)} - \left[J^{(k)}\right]^{-1} g\left(X^{(k)}\right) \quad (3.27)$$

Step 4: Check whether the following convergence criterion is met or not:

$$\sqrt{\sum_{i=1}^{2}\left(X_i^{k+1} - X_i^k\right)^2} \; < \; \varepsilon \text{ or not.} \quad (3.28)$$

where, ε, is a specified tolerance value and is chosen here as 10^{-4}.

If the algorithm has converged, the solution will be $X^{(k+1)}$; else, proceed to Step 5.

Step 5: Update the iteration counter k to k+1 and continue at Step 2.

A schematic flow chart has been shown in Fig. 3.4.

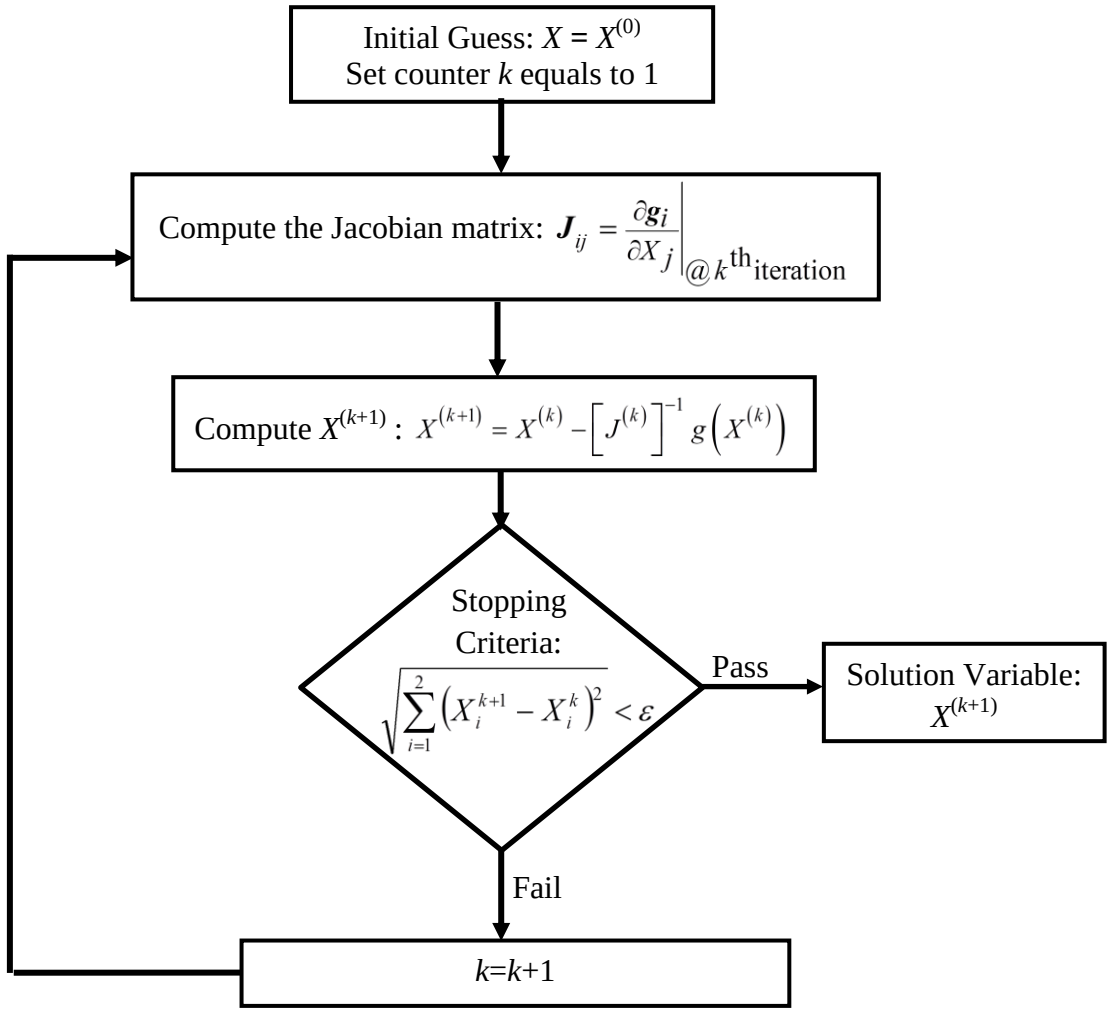

Fig. 3.4 Algorithm flowchart for the Newton-Raphson method.

3.4 RESULTS AND DISCUSSIONS

In this particular section, the findings related to four different cases are discussed in details.

3.4.1 Case 1: Homogeneous c-ϕ soil

Some typical homogeneous slopes are analyzed using the formulation derived by using the calculus of variation. The cohesion (c=5 kN/m^2), the unit weight of soil (γ=20 kN/m^3) and the height of the slope (h=10m) are maintained to be the same for all the cases. The critical factor of safety is calculated for different combinations of ϕ and β corresponding to varying k_h and k_v. The slope inclination angle (β) is varied within the range of 20º to 90º with a 5º interval. For each specific value of β, (i) three different internal friction angle, namely, 35º, 40º, and 45º are chosen. The magnitude of k_h is kept equal to 0.1, 0.2, and, 0.3 and corresponding to each k_h the vertical seismic coefficient k_v is varied as 0, 0.5k_h and k_h.

Table 3.7 shows the typical results of critical factor of safety for slopes with different ϕ and β and subjected to different combinations of horizontal and vertical seismic forces. The results are presented for four different values of β, namely, 20º, 30º, 40º and 50º.

Fig. 3.5 depicts the variation of critical factor of safety with k_h for different values of k_v/k_h. The graphs present the critical slip surface for different values of friction angle corresponding to four different value of β -- 25º, 35º, 55º and 65º. It is clearly observed from the obtained solutions that the critical factor of safety decreases with increase in horizontal and vertical seismic acceleration coefficient.

For an example, for β=25º and ϕ=35º, when the value of k_h increases from 0 to 0.1, F_s reduces by 21% and for the same slope F_s reduces by 34% when the value of k_h increases from 0 to 0.2. It is also noticed that F_s reduces with (i) increase in β and (ii) decrease in ϕ. For k_h =0.2, k_v = 0.5k_h and β=25º, F_s improves by 18% with the increase in ϕ from 40º to 45º. Reduction of the slope angle further improves the stability of the

slope. The critical factor of safety increases by 25% with the decrease of angle of slope from 35º to 25º for ϕ=45º soil and k_h=k_v=0.2.

Table 3.7 Critical factor of safety for different slopes corresponding to different seismic coefficients

		β=20^0			β=30^0			β=40^0			β=50^0		
k_h	ϕ / k_v	35^0	40^0	45^0	35^0	40^0	45^0	35^0	40^0	45^0	35^0	40^0	45^0
0	0	2.06	2.44	2.88	1.36	1.60	1.88	1.00	1.17	1.36	0.78	0.90	1.04
0.10	0.00	1.57	1.86	2.20	1.11	1.31	1.53	0.84	0.98	1.14	0.66	0.76	0.87
	0.05	1.55	1.84	2.17	1.10	1.30	1.52	0.83	0.97	1.13	0.65	0.75	0.86
	0.10	1.54	1.82	2.15	1.09	1.29	1.51	0.82	0.96	1.12	0.64	0.74	0.85
0.20	0.00	1.26	1.50	1.77	0.93	1.09	1.28	0.71	0.83	0.96	0.56	0.64	0.73
	0.10	1.22	1.44	1.70	0.91	1.07	1.25	0.70	0.82	0.95	0.55	0.63	0.72
	0.20	1.17	1.38	1.63	0.88	1.03	1.21	0.69	0.80	0.92	0.54	0.62	0.71
0.30	0.00	1.06	1.25	1.48	0.80	0.94	1.10	0.62	0.72	0.83	0.48	0.55	0.62
	0.15	0.98	1.16	1.37	0.75	0.88	1.04	0.60	0.68	0.79	0.46	0.53	0.60
	0.30	0.89	1.05	1.24	0.70	0.82	0.96	0.56	0.64	0.74	0.44	0.50	0.57

Fig. 3.6 illustrates the shape of the critical slip surface for β =60º and 80º with different combination of k_h and k_v. The volume of soil within the failure surface decreases as the strength of the soil (ϕ) increases. This feature is being observed irrespective of all slope angles. The shape of the slip surfaces changes significantly as the geometric profile of the slope changes. The figure also gives an impression that incorporation of the seismic forces increase the volume within the critical slip surface.

3.4.2 Case 2: Non-homogeneous undrained cohesive soil (ϕ_u=0°)

Some typical non-homogeneous clayey slopes are analyzed by using the formulation derived in the preceding section. The solutions are presented in the form of the critical factor of safety (F_s). The height of the slope (h), the unit weight of soil (γ) are to be maintained

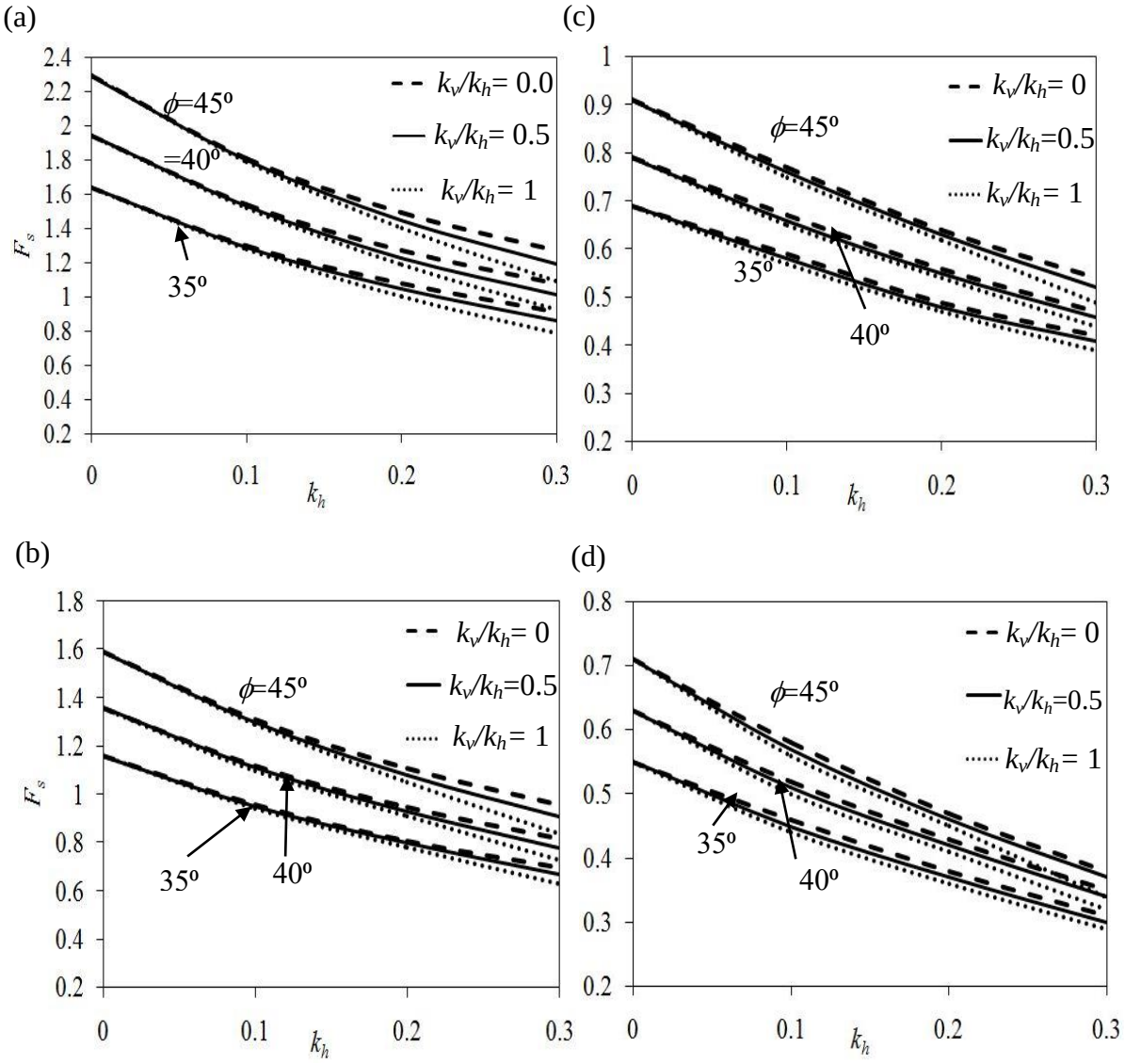

Fig. 3.5 Variation of critical factor of safety with k_h for: (a) β=25^0; (b) β=35^0; (c) β=55^0; (d) β=65^0.

identically for all cases. The critical factor of safety is evaluated for different combinations of cohesion coefficient (λ) and slope inclination angle (β) corresponding to varying k_h and k_v. The value of β has been varied within the range of 20^o to 90^o at an interval of 5^o. Three different values of λ, namely, 0, 1.5, and, 3.0 are chosen for each specific value of β. The magnitude of k_h is considered as 0.0, 0.1, 0.2, and, 0.3. For these values of k_h, corresponding magnitudes of k_v are 0, 0.5k_h, and k_h.

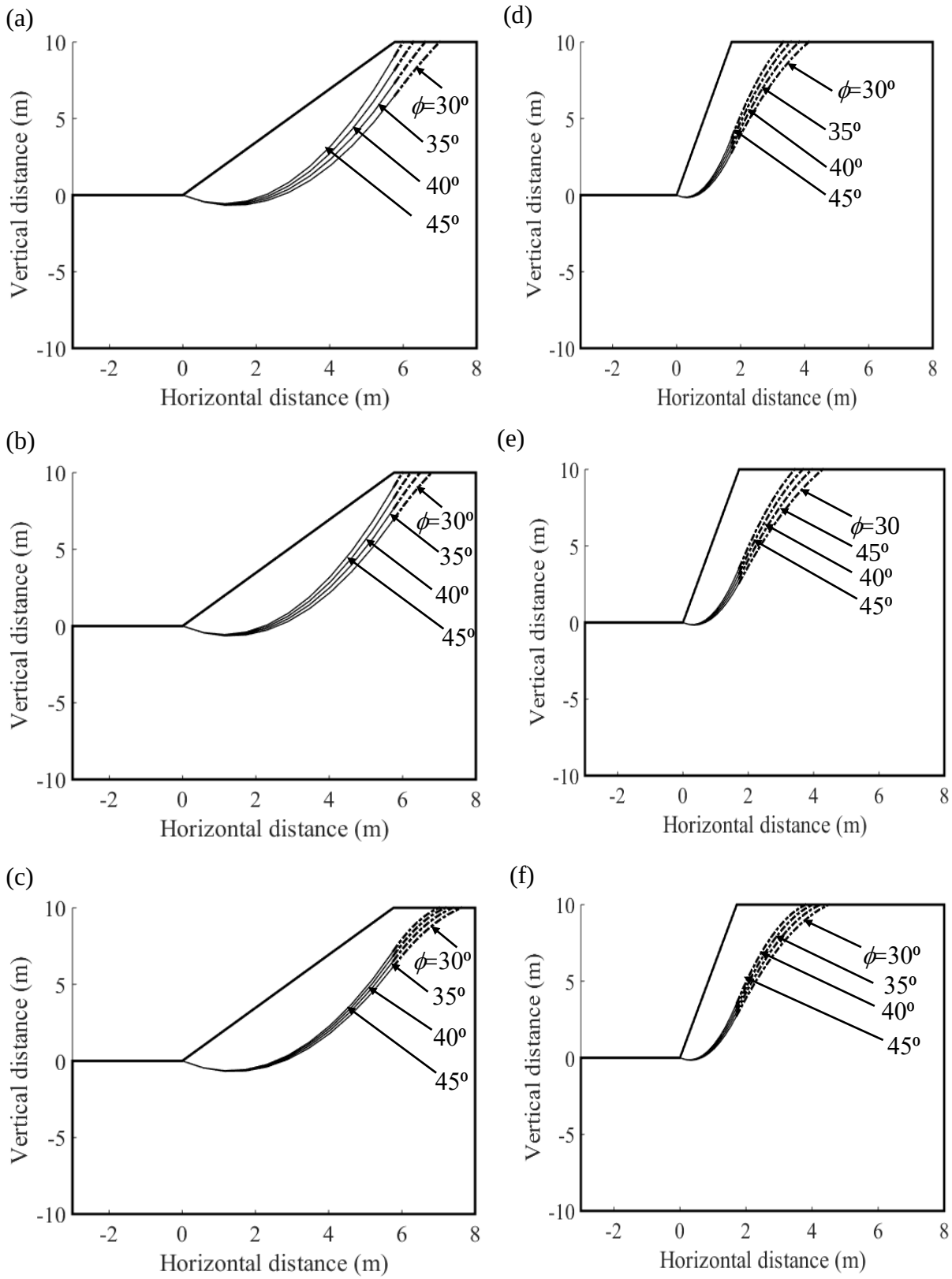

Fig. 3.6 Form of the critical slip surfaces for: (a) β=60^0, k_h=k_v=0; (b) β=60^0, k_h=0.3,k_v=0 ; (c) β=60^0, k_h=k_v=0.3; (d) β=80^0, k_h=k_v=0; (e) β=80^0, k_h=0.3, k_v=0; and (f) β=80^0, k_h=k_v=0.3.

Table 3.8 depicts the typical result of F_s of non-homogeneous soil slopes for a different combination of λ, β subjected to the different magnitude of k_h and k_v. The results are presented for four different values of β, namely, 45^o, 55^o, 65^o, and 75^o. Fig. 3.7 shows the variation of F_s with k_h for different values of k_v/k_h. The graphs represent the variation of F_s values for different combination λ values corresponding to four distinct values of β, namely, 20^o, 30^o, 40^o, and 50^o. It is clearly noticed from the obtained solutions that the magnitude F_s decreases with the increase in k_h and k_v values.

Table 3.8 F_s for different slopes corresponding to different seismic coefficients

		$\beta=45^o$			$\beta=55^o$			$\beta=65^o$			$\beta=75^o$		
k_h	λ / k_v	0.0	1.5	3.0	0.0	1.5	3.0	0.0	1.5	3.0	0.0	1.5	3.0
0	0	0.50	1.25	2.0	0.50	1.25	2.0	0.50	1.25	2.0	0.50	1.25	2.0
0.10	0.00	0.48	1.20	1.75	0.47	1.17	1.88	0.46	1.14	1.83	0.44	1.11	1.78
	0.05	0.46	1.14	1.83	0.45	1.12	1.80	0.44	1.09	1.75	0.43	1.06	1.70
	0.10	0.44	1.09	1.92	0.43	1.07	1.72	0.42	1.05	1.68	0.41	1.02	1.64
0.20	0.00	0.43	1.10	1.76	0.42	1.05	1.68	0.40	1.00	1.60	0.37	0.94	1.50
	0.10	0.41	1.02	1.63	0.39	0.98	1.57	0.37	0.93	1.49	0.35	0.88	1.41
	0.20	0.38	0.95	1.52	0.37	0.91	1.46	0.35	0.88	1.40	0.33	0.83	1.33
0.30	0.00	0.37	0.91	1.46	0.34	0.85	1.36	0.31	0.78	1.26	0.29	0.71	1.14
	0.15	0.35	0.87	1.39	0.33	0.82	1.31	0.30	0.76	1.22	0.28	0.70	1.12
	0.30	0.32	0.81	1.29	0.31	0.77	1.23	0.29	0.72	1.16	0.27	0.67	1.08

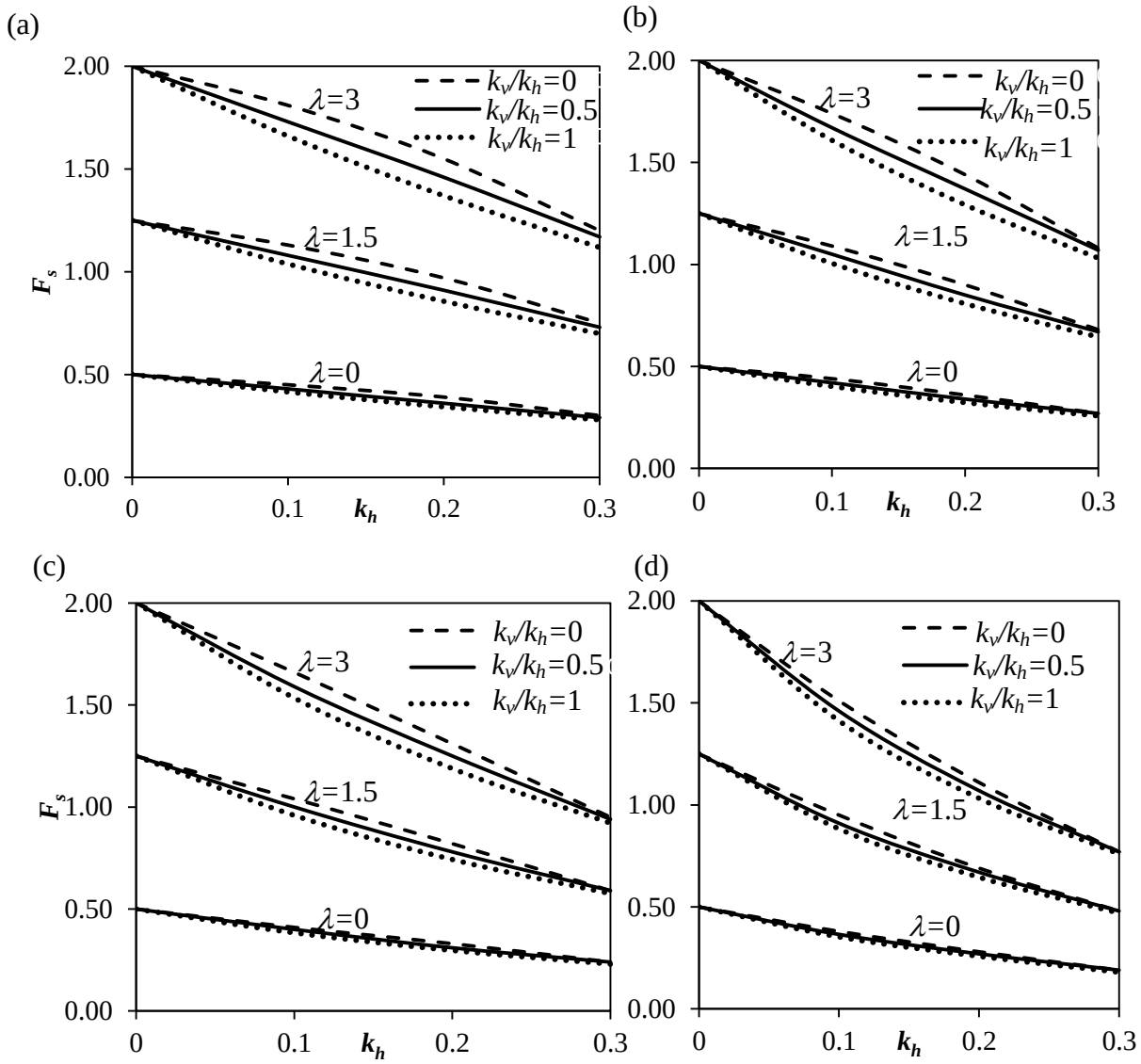

Fig. 3.7 Variation of critical factor of safety (F_s) with k_h for: (a) β=20º; (b) β=30º; (c) β=40º; (d) β=50º.

For example, for β =20º and λ=3, when the magnitude of k_h increases from 0 to 0.1, F_s reduce by 10.50%, and for the same slope, the reduction of F_s is 66.67% when the magnitude of k_h increases from 0 to 0.3. It is also observed that F_s reduce with (i) increase in β and (ii) decrease in λ. For k_h =0.3, k_v = 0.5k_h and β=20º, F_s improves by 75.21% with the increase in λ from 0 to 3. The stability of the slope further improves by reducing β. F_s increases by 32.14% with the decrease of β from 50º to 20º for λ=3 and k_h=k_v=0.3.

Fig. 3.8 illustrates the shape of the critical slip surface for β=20^o, 40^o, 60^o, and 80^o with a different combination of k_h. The magnitude of λ and k_v are kept 3 and 0, respectively. The shape of the critical slip surface changes markedly with the geometric profile of the slope. Moreover, the shape of critical slip surface is dependent on the unknown end point x_3, a variable influenced by slope height (h), slope angle (β), seismic acceleration coefficients (k_h, k_v). When slope height and seismic acceleration coefficients remain unchanged, the horizontal extent of endpoint x_3 is more pronounced for flatter slopes than for steeper ones. Consequently, the critical slip surface exhibits a considerably deeper-seated nature on flatter slopes in contrast to steep slopes. The figure also gives the impression that the volume of soil within the critical slip surface increases with the increment of the magnitude of seismic forces.

3.4.3 Case 3: Two layered cohesive-frictional soil

In the present analysis, some typical two layered slopes are analyzed using the formulations derived in the previous section. The solutions are presented in the form of non-dimensional stability number as expressed in Table 3.6 for Case 3. It is to be observed that for the non-seismic case, the stability number for non-frictional soil will be equal to $c_1/(4c_2)$ and this further resorted to 0.25 for homogenous undrained cohesive soil as mentioned in the work of Revilla and Castillo (1977). The unit weight of soil and the height of the slope are maintained to be the same for all the cases. The stability number is calculated for different combinations of c_1/c_2 ($=\alpha$) and β corresponding to varying k_h and k_v. The slope inclination angle (β) is varied within the range of 45° to 75° with a 10° interval.

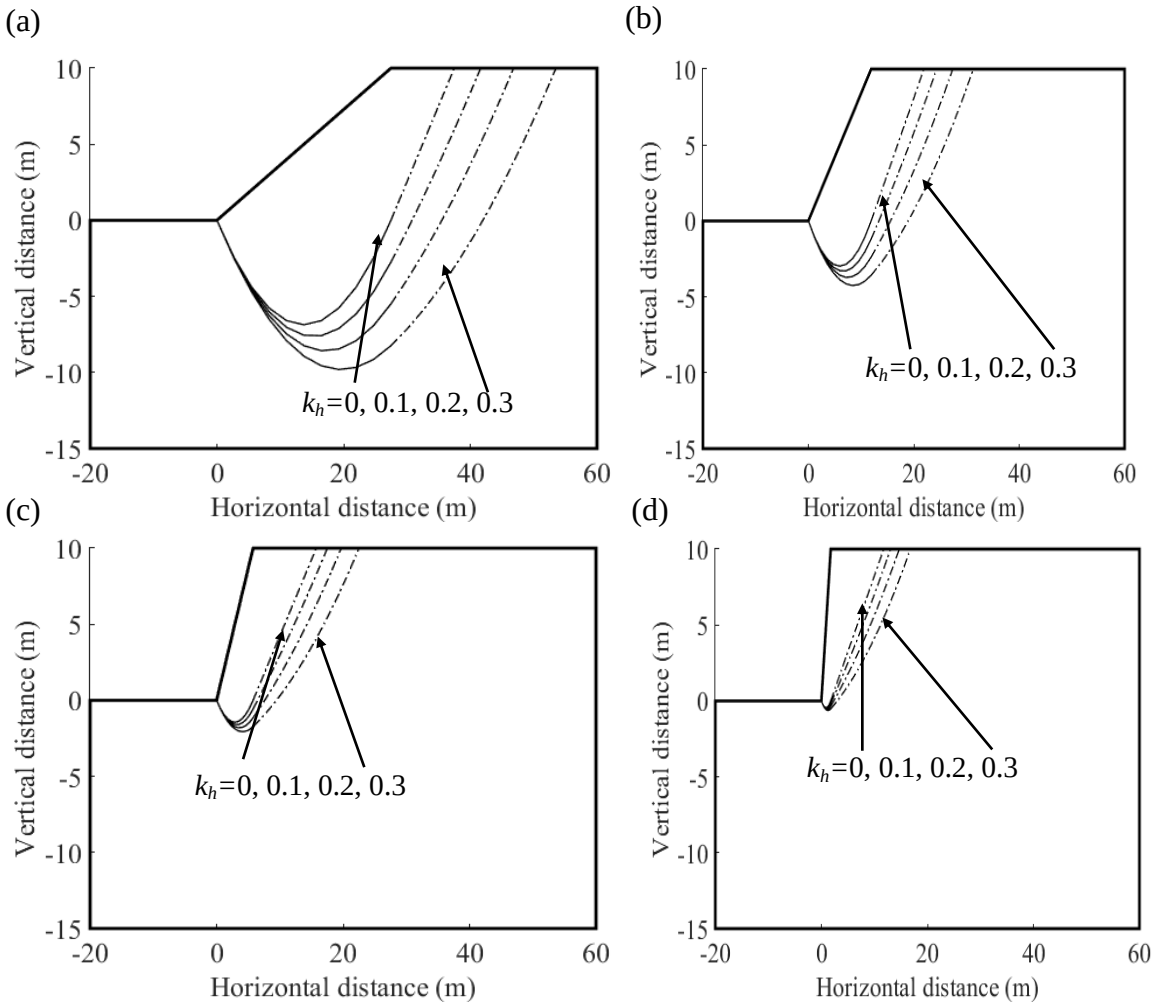

Fig. 3.8 Form of the critical slip surfaces for: (a) β=20^o, λ=3, k_v=0; (b) β=40^o, λ=3, k_v=0; (c) β=60^o, λ=3, k_v=0 (d) β=80^o, λ=3, k_v=0.

For each specific value of β, c_1/c_2 is varied from 0.2 to 0.8 corresponding to two different cases: (i) Case A (ϕ_1=18°,ϕ_2=30°) and (ii) Case B (ϕ_1=ϕ_2=30°). The magnitude of k_h is kept equal to 0.1, 0.2, and, 0.3 and corresponding to each k_h the vertical seismic coefficient k_v is varied as 0, 0.5 k_h and k_h. The top layer is considered to be weaker than the bottom layer and the slope angle is considered to be greater than 45°, and, hence, according to the literatures (Kumar & Samui, 2006; Lim et al., 2015; Sazzad, et al. 2017) the soil will fail by developing toe failure surface (x0=0). Figs. 3.9 and 3.10 shows the variation of stability number with k_h for different values of k_v/k_h and c_1/c_2

corresponding to four different values of β, namely, 45°, 55°, 65° and 75°; Fig. 3.9 depicts the graph for Case A and Fig. 3.10 shows the graph for Case B. It is clearly observed from the figures that for a certain c_1/c_2 ratio, the stability number increases with increase in horizontal seismic acceleration coefficient. The rate of increment in N, or, in other words, the rate of decrement in F_s seems to increase as the k_h increases. It is further noticed that the stability number increases with (i) increase in c_1/c_2, (ii) decrease in ϕ_1/ϕ_2, and, (iii) increase in β.

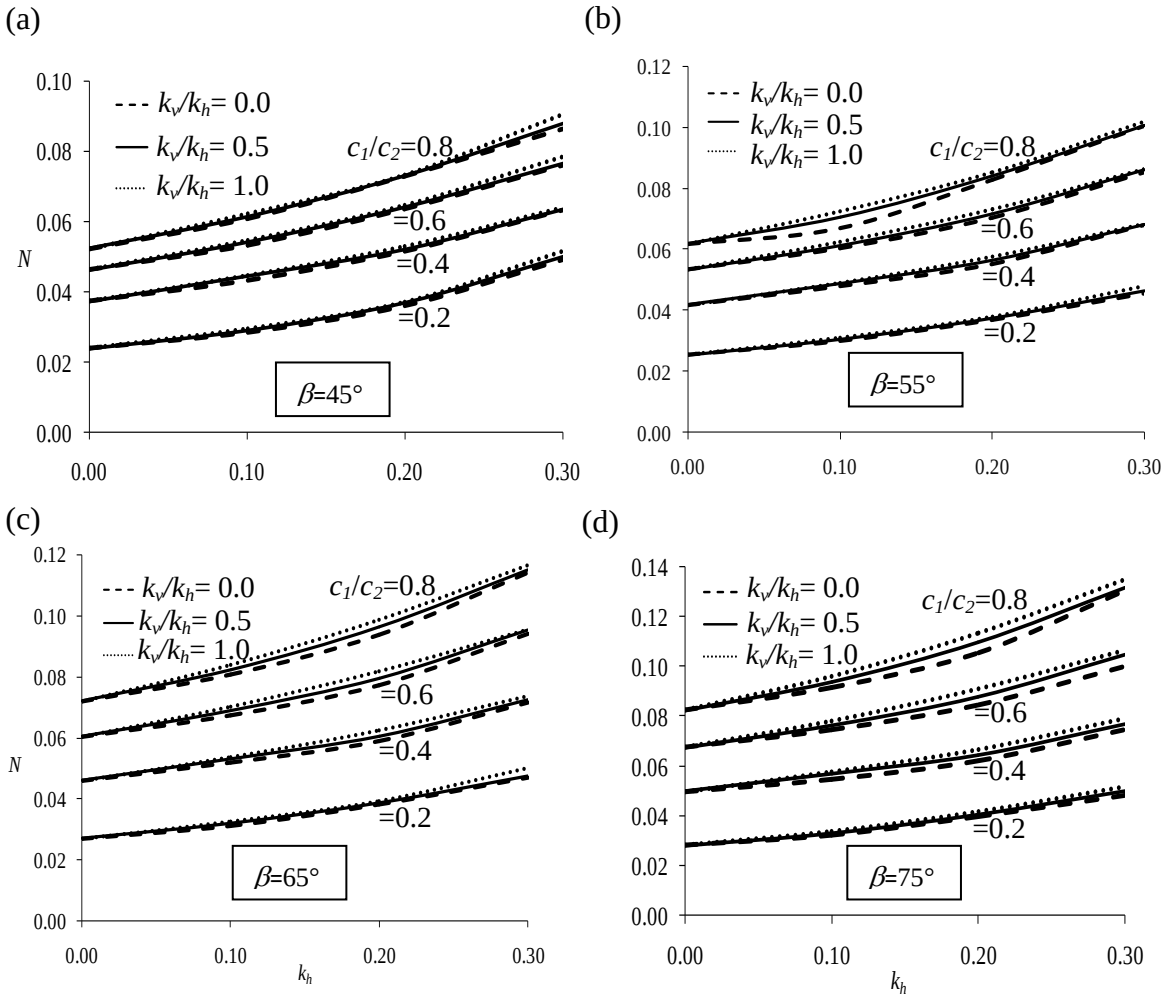

Fig. 3.9 Variation of stability number with k_h for Case A soil with: (a) β=45°; (b) β=55°; (c) β=65°; (d) β=75°.

In Figs. 3.9 and 3.10, the significant increment in the magnitude of the stability number is observed as k_v/k_h enhances, particularly noticeable in the context of steeper slopes. The figures also suggest that the influence of vertical seismic acceleration is not significant as its horizontal counterpart. The impact of k_v is noticeable for the steep slopes.

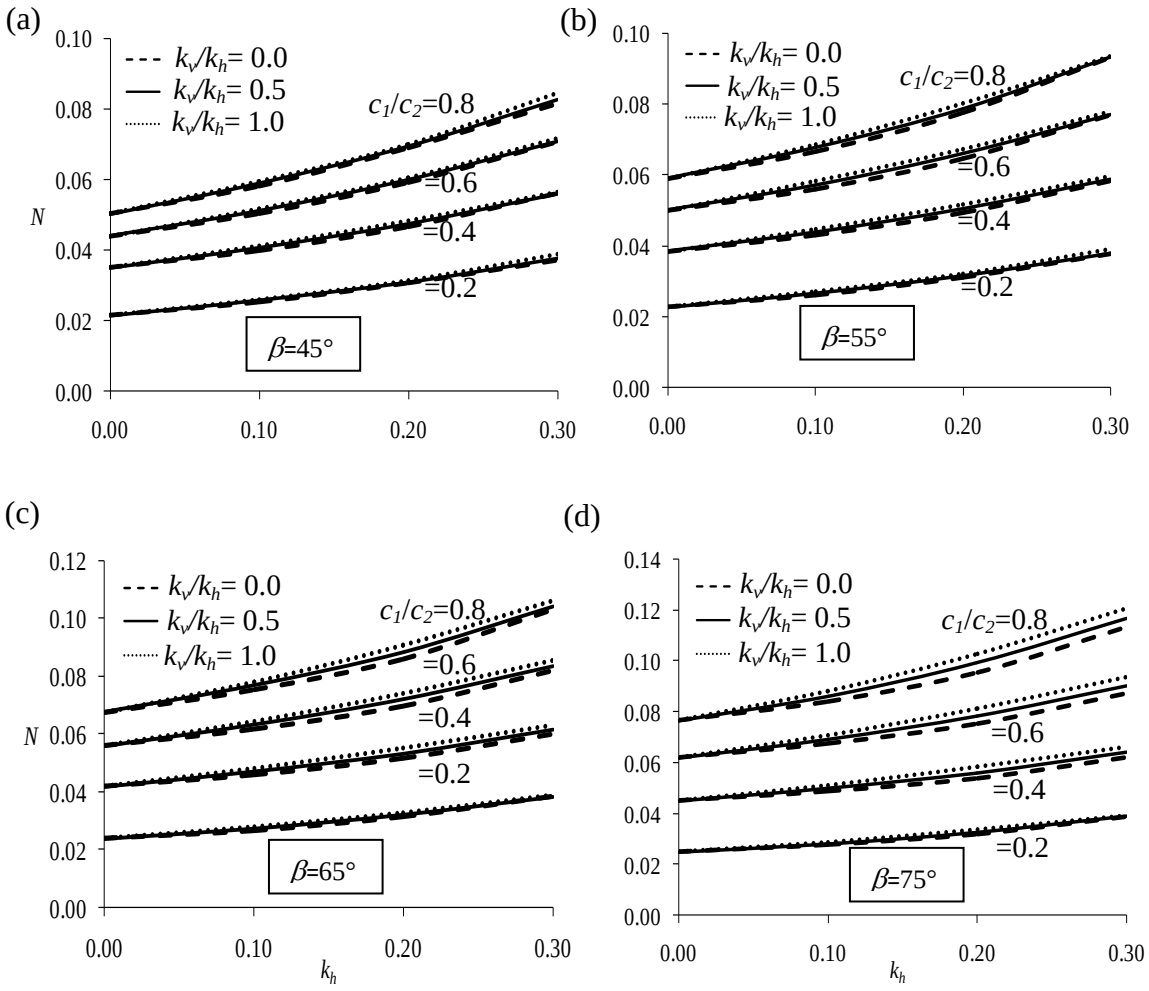

Fig. 3.10 Variation of stability number with k_h for Case B soil with: (a) β=45°; (b) β=55°; (c) β=65°; (d) β=75°.

Fig. 3.11 illustrates the shape of the critical slip surface for β =55° and 75° with different combination of k_h and k_v. The shape of the slip surfaces changes significantly as the geometric profile of the slope changes. The figure also shows that the volume of soil within the critical slip surface increases as the ratio of c_1/c_2 decreases. The

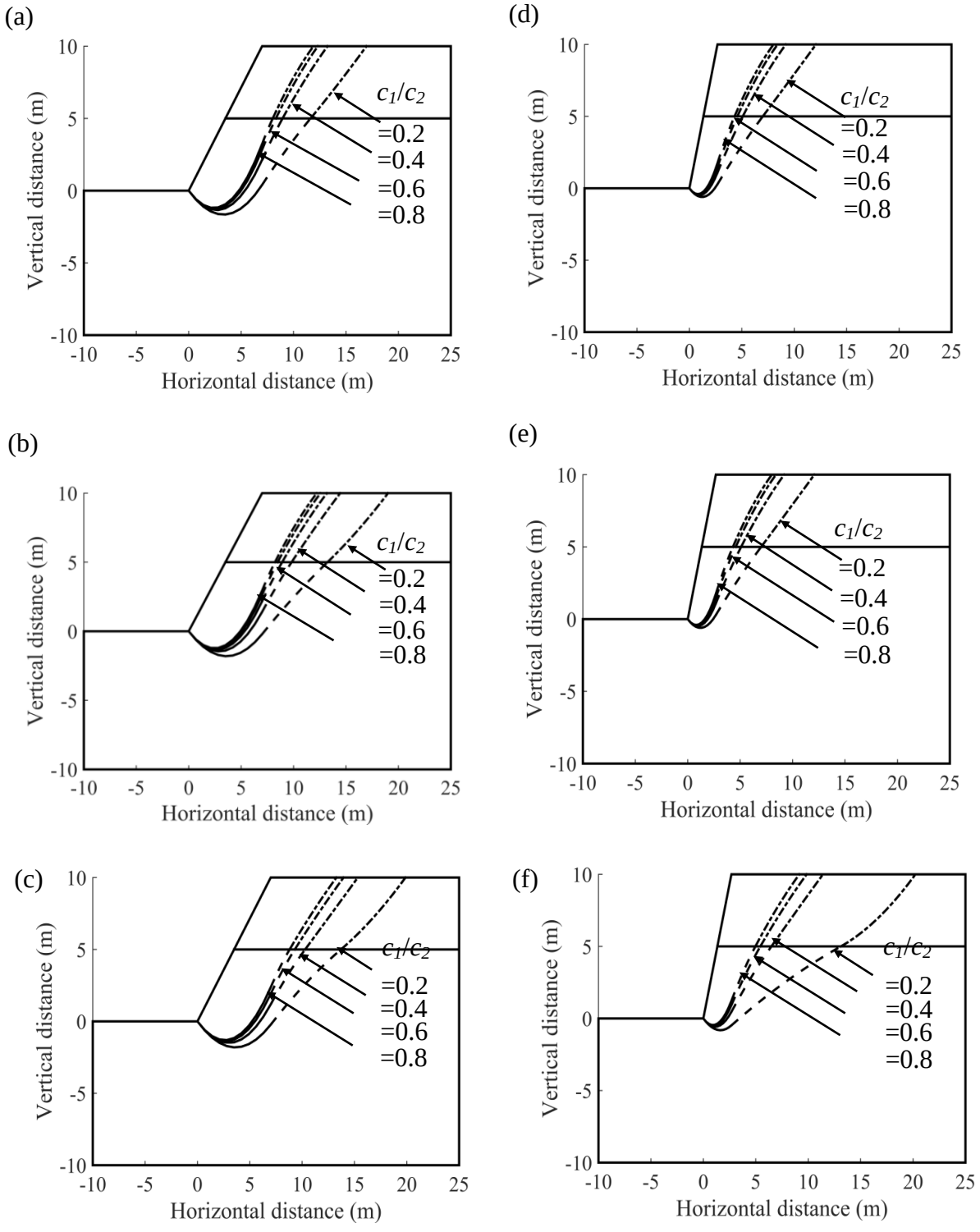

Fig. 3.11 Form of the critical slip surfaces for: (a) β=55°, k_h=k_v=0; (b) β=55°, k_h=0.3,k_v=0 ; (c) β=55°, k_h=k_v=0.3; (d) β=75°, k_h=k_v=0; (e) β=75°, k_h=0.3, k_v=0; and (f) β=75°, k_h=k_v=0.3 subjected to ϕ_1=18° and ϕ_2=30°.

horizontal extent of the failure surface for c_1/c_2=0.2 is quite higher than the other considered c_1/c_2 ratio. The figure also gives an impression that the incorporation of the seismic forces increases the size of the failure surfaces.

3.4.4 Case 4: Homogeneous *c*-ϕ soil underlain by non-homogeneous clays

Some typical two layered slopes, consisting of *c*-ϕ soil (top layer) and non-homogeneous undrained cohesive soil (ϕ_u=0^o) with varying cohesion along with depth (bottom layer) are analysed by using the formulation depicted in Section 3.3. In all cases the height of the slope (h) and the unit weight of soil (γ) have been maintained identically. The critical factor of safety is estimated for different combinations of slope inclination angle (β), cohesion coefficient (λ), angle of internal friction (ϕ), and top layer thickness coefficient (α_1) corresponding to varying k_h and k_v. The value of β has been varied from 20^o to 90^o at an interval of 5^o. Three different values of λ such as 0, 1.5, and, 3 are chosen for each specific value of β. The magnitude of k_h is taken as 0.0, 0.1, 0.2, and, 0.3. For each value of k_h, the magnitudes of k_v are chosen as 0, 0.5k_h, and k_h. The value of angle of internal friction (ϕ) is adopted as 35^o, 40^o, and 45^o. All these input parameters are chosen by studying previous literatures (Koppula 1984; Choudhury et al. 2007; Griffiths and Yu 2015; Li et al. 2018) to cover wide possible ranges of various combinations of parameters in the field.

Tables 3.9-3.11 display the computed value of F_s for various soil slopes (λ, β, ϕ, and α_1) subjected to different combinations of k_h and k_v; Tables 3.9, 3.10, and 3.11 correspond to ϕ = 35^o, 40^o and 45^o, respectively. The thickness of the top layer is varied between 20%-80% of the slope height. From Tables 3.9-3.11, it has been noticed that the influence of β on the value of F_s is more visible for the pseudo-static case. For the

Table 3.9 The proposed stability chart corresponding to ϕ=35°

λ	k_h	k_v	α_1=0.2			α_1=0.4			α_1=0.5			α_1=0.6			α_1=0.8		
			β=25°	β=45°	β=65°	β=25°	β=45°	β=65°	β=25°	β=45°	β=65°	β=25°	β=45°	β=65°	β=25°	β=45°	β=65°
0	0	0	0.389	0.389	0.389	0.460	0.460	0.460	0.490	0.490	0.490	0.518	0.518	0.518	0.568	0.568	0.568
	0.1	0	0.380	0.364	0.335	0.454	0.437	0.405	0.486	0.468	0.435	0.515	0.496	0.461	0.567	0.547	0.510
		0.05	0.366	0.352	0.325	0.442	0.423	0.394	0.475	0.454	0.423	0.506	0.481	0.449	0.560	0.531	0.496
		0.10	0.363	0.341	0.316	0.439	0.411	0.384	0.470	0.441	0.412	0.498	0.470	0.438	0.549	0.521	0.484
	0.2	0	0.354	0.334	0.288	0.425	0.410	0.357	0.456	0.440	0.386	0.488	0.467	0.412	0.544	0.516	0.459
		0.10	0.342	0.317	0.276	0.421	0.389	0.343	0.456	0.419	0.370	0.483	0.446	0.396	0.533	0.496	0.441
		0.20	0.336	0.301	0.266	0.417	0.376	0.330	0.448	0.408	0.356	0.477	0.438	0.381	0.529	0.490	0.424
	0.3	0	0.323	0.298	0.244	0.395	0.371	0.312	0.425	0.399	0.340	0.454	0.426	0.366	0.506	0.473	0.411
		0.15	0.315	0.284	0.237	0.393	0.356	0.302	0.425	0.386	0.328	0.452	0.413	0.352	0.501	0.462	0.395
		0.30	0.295	0.269	0.228	0.367	0.337	0.290	0.397	0.365	0.315	0.424	0.390	0.338	0.473	0.436	0.379
1.5	0	0	0.972	0.972	0.972	1.149	1.149	1.149	1.225	1.225	1.225	1.294	1.294	1.294	1.419	1.419	1.419
	0.1	0	0.930	0.892	0.822	1.101	1.059	0.983	1.172	1.129	1.050	1.236	1.193	1.111	1.352	1.306	1.220
		0.05	0.898	0.863	0.798	1.067	1.029	0.958	1.137	1.098	1.025	1.200	1.160	1.085	1.314	1.272	1.192
		0.10	0.869	0.837	0.777	1.035	1.000	0.935	1.104	1.068	1.000	1.167	1.130	1.060	1.279	1.240	1.166
	0.2	0	0.864	0.796	0.688	1.026	0.953	0.836	1.091	1.017	0.895	1.150	1.074	0.949	1.253	1.174	1.042
		0.10	0.819	0.761	0.665	0.978	0.915	0.811	1.043	0.978	0.870	1.101	1.035	0.923	1.204	1.134	1.016
		0.20	0.778	0.727	0.642	0.934	0.879	0.786	0.998	0.941	0.844	1.055	0.997	0.896	1.157	1.095	0.988
	0.3	0	0.766	0.683	0.565	0.917	0.828	0.699	0.976	0.885	0.752	1.027	0.935	0.798	1.116	1.021	0.878
		0.15	0.735	0.664	0.559	0.885	0.808	0.692	0.945	0.866	0.745	0.998	0.916	0.792	1.089	1.005	0.874
		0.30	0.697	0.637	0.545	0.845	0.779	0.676	0.904	0.836	0.729	0.957	0.887	0.776	1.049	0.976	0.858
3.0	0	0	1.555	1.555	1.555	1.839	1.839	1.839	1.960	1.960	1.960	2.070	2.070	2.070	2.271	2.271	2.271
	0.1	0	1.457	1.398	1.289	1.705	1.643	1.527	1.807	1.743	1.625	1.900	1.834	1.713	2.063	1.995	1.868
		0.05	1.409	1.355	1.254	1.657	1.599	1.491	1.758	1.699	1.589	1.850	1.790	1.676	2.013	1.950	1.831
		0.10	1.365	1.315	1.222	1.611	1.558	1.457	1.712	1.657	1.554	1.804	1.747	1.641	1.966	1.907	1.796
	0.2	0	1.313	1.213	1.053	1.519	1.418	1.251	1.600	1.497	1.329	1.671	1.568	1.397	1.792	1.688	1.515
		0.10	1.255	1.168	1.025	1.467	1.377	1.226	1.551	1.459	1.305	1.625	1.532	1.376	1.752	1.658	1.497
		0.20	1.199	1.123	0.994	1.414	1.334	1.197	1.499	1.417	1.277	1.575	1.492	1.349	1.707	1.621	1.473
	0.3	0	1.113	1.000	0.842	1.274	1.172	1.015	1.341	1.240	1.081	1.400	1.298	1.139	1.497	1.396	1.241
		0.15	1.094	0.993	0.837	1.274	1.165	1.009	1.333	1.225	1.078	1.382	1.288	1.138	1.489	1.395	1.235
		0.30	1.054	0.967	0.831	1.244	1.153	1.001	1.317	1.225	1.062	1.381	1.276	1.114	1.463	1.360	1.200

Table 3.10 The proposed stability chart corresponding to ϕ=40°

λ	k_h	k_v	α_1=0.2			α_1=0.4			α_1=0.5			α_1=0.6			α_1=0.8		
			β=25°	β=45°	β=65°	β=25°	β=45°	β=65°	β=25°	β=45°	β=65°	β=25°	β=45°	β=65°	β=25°	β=45°	β=65°
0	0	0	0.404	0.404	0.404	0.484	0.484	0.484	0.517	0.517	0.517	0.548	0.548	0.548	0.610	0.610	0.610
	0.1	0	0.396	0.380	0.351	0.480	0.462	0.429	0.514	0.496	0.461	0.546	0.527	0.491	0.604	0.583	0.544
		0.05	0.382	0.368	0.341	0.469	0.448	0.417	0.505	0.481	0.449	0.539	0.511	0.478	0.599	0.566	0.530
		0.10	0.381	0.356	0.331	0.464	0.435	0.406	0.498	0.470	0.437	0.529	0.501	0.466	0.585	0.558	0.517
	0.2	0	0.370	0.351	0.303	0.450	0.434	0.380	0.487	0.467	0.411	0.522	0.497	0.440	0.585	0.551	0.492
		0.10	0.358	0.333	0.291	0.449	0.413	0.365	0.483	0.446	0.395	0.513	0.477	0.423	0.568	0.531	0.473
		0.20	0.355	0.317	0.280	0.442	0.402	0.351	0.477	0.437	0.381	0.509	0.470	0.407	0.565	0.527	0.455
	0.3	0	0.339	0.315	0.259	0.419	0.394	0.335	0.454	0.425	0.366	0.486	0.454	0.394	0.543	0.506	0.444
		0.15	0.333	0.300	0.252	0.418	0.380	0.323	0.452	0.413	0.352	0.482	0.443	0.378	0.536	0.497	0.426
		0.30	0.311	0.284	0.242	0.391	0.359	0.310	0.424	0.390	0.338	0.454	0.418	0.363	0.507	0.469	0.408
1.5	0	0	1.011	1.011	1.011	1.210	1.210	1.210	1.293	1.293	1.293	1.370	1.370	1.370	1.509	1.509	1.509
	0.1	0	0.971	0.933	0.861	1.164	1.122	1.043	1.244	1.200	1.118	1.317	1.271	1.186	1.446	1.398	1.307
		0.05	0.939	0.903	0.837	1.129	1.090	1.017	1.207	1.167	1.090	1.279	1.237	1.158	1.406	1.361	1.277
		0.10	0.909	0.876	0.815	1.096	1.060	0.992	1.173	1.136	1.065	1.244	1.205	1.131	1.369	1.327	1.249
	0.2	0	0.909	0.839	0.728	1.093	1.018	0.894	1.168	1.090	0.961	1.235	1.154	1.021	1.352	1.267	1.127
		0.10	0.862	0.802	0.703	1.042	0.977	0.867	1.116	1.047	0.933	1.182	1.111	0.992	1.298	1.223	1.097
		0.20	0.818	0.766	0.679	0.995	0.938	0.840	1.067	1.007	0.905	1.132	1.070	0.963	1.246	1.180	1.067
	0.3	0	0.815	0.728	0.605	0.989	0.895	0.757	1.057	0.959	0.816	1.117	1.017	0.869	1.219	1.116	0.960
		0.15	0.779	0.706	0.596	0.951	0.870	0.746	1.019	0.935	0.806	1.079	0.992	0.859	1.184	1.093	0.951
		0.30	0.738	0.676	0.580	0.906	0.837	0.727	0.973	0.901	0.786	1.033	0.958	0.839	1.138	1.058	0.931
3.0	0	0	1.617	1.617	1.617	1.936	1.936	1.936	2.070	2.070	2.070	2.193	2.193	2.193	2.414	2.414	2.414
	0.1	0	1.524	1.464	1.352	1.808	1.744	1.623	1.925	1.858	1.733	2.030	1.961	1.833	2.215	2.143	2.009
		0.05	1.475	1.420	1.317	1.757	1.697	1.585	1.873	1.811	1.695	1.977	1.913	1.794	2.161	2.094	1.969
		0.10	1.430	1.379	1.283	1.709	1.654	1.549	1.824	1.766	1.658	1.927	1.868	1.757	2.110	2.048	1.930
	0.2	0	1.387	1.284	1.117	1.630	1.522	1.346	1.725	1.616	1.436	1.809	1.698	1.515	1.952	1.840	1.652
		0.10	1.325	1.235	1.086	1.571	1.476	1.317	1.669	1.571	1.408	1.755	1.656	1.489	1.904	1.802	1.628
		0.20	1.265	1.187	1.054	1.513	1.428	1.284	1.611	1.525	1.376	1.699	1.610	1.457	1.851	1.759	1.599
	0.3	0	1.193	1.074	0.902	1.391	1.272	1.103	1.463	1.351	1.179	1.532	1.421	1.246	1.649	1.537	1.360
		0.15	1.167	1.061	0.901	1.381	1.272	1.093	1.462	1.345	1.171	1.525	1.407	1.240	1.631	1.528	1.359
		0.30	1.122	1.030	0.888	1.343	1.246	1.092	1.429	1.330	1.165	1.503	1.403	1.227	1.626	1.510	1.329

Table 3.11 The proposed stability chart corresponding to ϕ=45°

λ	k_h	k_v	α_1=0.2			α_1=0.4			α_1=0.5			α_1=0.6			α_1=0.8		
			β=25°	β=45°	β=65°	β=25°	β=45°	β=65°	β=25°	β=45°	β=65°	β=25°	β=45°	β=65°	β=25°	β=45°	β=65°
0	0	0	0.421	0.421	0.421	0.510	0.510	0.510	0.547	0.547	0.547	0.581	0.581	0.581	0.642	0.642	0.642
	0.1	0	0.414	0.398	0.367	0.507	0.488	0.454	0.545	0.526	0.490	0.580	0.560	0.522	0.644	0.622	0.581
		0.05	0.410	0.385	0.357	0.497	0.473	0.442	0.538	0.510	0.477	0.574	0.544	0.509	0.640	0.604	0.566
		0.10	0.400	0.373	0.347	0.490	0.462	0.430	0.528	0.500	0.465	0.562	0.535	0.496	0.628	0.597	0.552
	0.2	0	0.387	0.369	0.320	0.479	0.460	0.404	0.521	0.496	0.439	0.559	0.529	0.471	0.624	0.588	0.527
		0.10	0.377	0.350	0.307	0.475	0.439	0.389	0.512	0.475	0.422	0.546	0.509	0.452	0.606	0.568	0.507
		0.20	0.376	0.334	0.295	0.469	0.429	0.374	0.507	0.468	0.406	0.542	0.504	0.436	0.604	0.567	0.488
	0.3	0	0.356	0.333	0.276	0.446	0.418	0.359	0.485	0.453	0.393	0.520	0.485	0.423	0.583	0.542	0.478
		0.15	0.351	0.317	0.267	0.444	0.406	0.345	0.481	0.442	0.377	0.514	0.475	0.406	0.574	0.533	0.458
		0.30	0.328	0.300	0.257	0.416	0.383	0.332	0.452	0.417	0.362	0.485	0.448	0.390	0.544	0.503	0.439
1.5	0	0	1.053	1.053	1.053	1.275	1.275	1.275	1.367	1.367	1.367	1.452	1.452	1.452	1.605	1.605	1.605
	0.1	0	1.017	0.977	0.903	1.233	1.188	1.106	1.322	1.275	1.190	1.402	1.355	1.265	1.546	1.495	1.400
		0.05	0.983	0.947	0.879	1.196	1.155	1.079	1.283	1.241	1.161	1.362	1.318	1.236	1.504	1.457	1.368
		0.10	0.957	0.918	0.856	1.166	1.124	1.053	1.250	1.208	1.134	1.325	1.284	1.207	1.464	1.421	1.338
	0.2	0	0.952	0.886	0.770	1.161	1.086	0.956	1.247	1.167	1.031	1.325	1.239	1.099	1.457	1.367	1.217
		0.10	0.908	0.846	0.744	1.111	1.042	0.927	1.193	1.121	1.000	1.267	1.192	1.067	1.397	1.318	1.183
		0.20	0.867	0.809	0.718	1.066	1.000	0.897	1.143	1.078	0.970	1.213	1.147	1.035	1.341	1.270	1.150
	0.3	0	0.862	0.776	0.647	1.060	0.965	0.818	1.141	1.038	0.884	1.211	1.104	0.944	1.329	1.216	1.047
		0.15	0.827	0.750	0.635	1.021	0.935	0.804	1.098	1.008	0.870	1.166	1.073	0.930	1.285	1.186	1.033
		0.30	0.783	0.718	0.617	0.971	0.898	0.782	1.046	0.969	0.848	1.114	1.034	0.906	1.231	1.146	1.009
3.0	0	0	1.685	1.685	1.685	2.039	2.039	2.039	2.188	2.188	2.188	2.323	2.323	2.323	2.567	2.567	2.567
	0.1	0	1.597	1.535	1.421	1.919	1.851	1.726	2.050	1.980	1.850	2.168	2.096	1.961	2.377	2.301	2.158
		0.05	1.547	1.490	1.384	1.865	1.803	1.686	1.995	1.930	1.809	2.112	2.045	1.919	2.319	2.248	2.115
		0.10	1.500	1.447	1.349	1.815	1.757	1.648	1.943	1.883	1.769	2.059	1.997	1.879	2.264	2.198	2.073
	0.2	0	1.466	1.359	1.186	1.747	1.634	1.447	1.857	1.741	1.549	1.955	1.836	1.640	2.122	2.000	1.796
		0.10	1.399	1.306	1.152	1.682	1.582	1.413	1.794	1.691	1.517	1.893	1.788	1.608	2.065	1.955	1.767
		0.20	1.337	1.255	1.117	1.619	1.530	1.377	1.731	1.639	1.480	1.831	1.736	1.573	2.004	1.905	1.733
	0.3	0	1.279	1.153	0.969	1.515	1.385	1.195	1.602	1.472	1.283	1.676	1.550	1.360	1.810	1.687	1.490
		0.15	1.245	1.134	0.967	1.494	1.377	1.191	1.589	1.470	1.274	1.671	1.546	1.349	1.799	1.669	1.485
		0.30	1.193	1.098	0.948	1.448	1.345	1.180	1.547	1.440	1.270	1.634	1.525	1.346	1.781	1.669	1.467

chosen combinations of input parameters, the extent of top layer always contributes towards the improvement of F_s for both static and pseudo-static case.

Tables 3.12 and 3.13 show the percentage enhancement of F_s due to increment of ϕ from 35^o to 40^o and 35^o to 45^o, respectively. It can be interpreted that irrespective of the bottom layer strength, top layer thickness, slope angle, and seismic conditions, the improvement of F_s is almost double for the case when ϕ changes from 35^o to 45^o in contrast to the case when ϕ changes from 35^o to 40^o. The strength improvement of the top layer zone is more beneficial in seismic prone area. For an instance, when ϕ changes from 35^o to 45^o correspond to $\beta=65^o$, α_1 =0.2, the 8% improvement of F_s for static loading ($k_h=k_v=0$) turns out to be 13% for-pseudo-static loading ($k_h=0.3$, $k_v=0$). Furthermore, when the top layer thickness is relatively shallower, improvement of top layer strength is more beneficial for the steep slope (e.g. $\beta=65^o$) than the gentle slope (e.g. $\beta=25^o$). The enhancement of the bottom layer cohesion and the extension of the top layer thickness further improve the stability. In a nutshell, improving the strength of the top layer becomes more effective for the steep slopes with high value of λ and α_1 subjected to extreme seismic loading. The percentage improvement of F_s corresponding to $\lambda=3$, $\alpha_1=0.8$, $k_h=k_v=0.3$, $\beta=65^o$ is reported to be high as 22.5% when top layer frictional strength changes from 35^o to 45^o.

To illustrate the combined effect of λ, β, α_1, k_h, k_v on F_s pictorially, Figs. 3.12 and 3.13 are drawn. This figures shows the variation of F_s with k_h corresponding to three λ's (0, 1.5, 3), four β's, three seismic coefficient ratios (k_v/k_h=0.0, 0.5, 1.0); Fig 3.12 correspond to $\alpha_1=0.2$ and Fig 3.13 correspond to $\alpha_1=0.6$. The F_s -k_h profile becomes more nonlinear with increase in λ values.

Table 3.12 The percentage improvement of F_s during the increment of ϕ from 35° to 40°

λ	k_h	k_v	α_1=0.2			α_1=0.5			α_1=0.8		
			β=25°	β=45°	β=65°	β=25°	β=45°	β=65°	β=25°	β=45°	β=65°
0	0	0	3.86	3.86	3.86	5.51	5.51	5.51	7.39	7.39	7.39
	0.1	0	4.21	4.40	4.78	5.76	5.98	5.98	6.53	6.58	6.67
		0.05	4.37	4.55	4.92	6.32	5.95	6.15	6.96	6.59	6.85
		0.1	4.96	4.40	4.75	5.96	6.58	6.07	6.56	7.10	6.82
	0.2	0	4.52	5.09	5.21	6.80	6.14	6.48	7.54	6.78	7.19
		0.1	4.68	5.05	5.43	5.92	6.44	6.76	6.57	7.06	7.26
		0.2	5.65	5.32	5.26	6.47	7.11	7.02	6.81	7.55	7.31
	0.3	0	4.95	5.70	6.15	6.82	6.52	7.65	7.31	6.98	8.03
		0.15	5.71	5.63	6.33	6.35	6.99	7.32	6.99	7.58	7.85
		0.3	5.42	5.58	6.14	6.80	6.85	7.30	7.19	7.57	7.65
1.5	0	0	4.01	4.01	4.01	5.55	5.55	5.55	6.34	6.34	6.34
	0.1	0	4.41	4.60	4.74	6.14	6.29	6.48	6.95	7.04	7.13
		0.05	4.57	4.63	4.89	6.16	6.28	6.34	7.00	7.00	7.13
		0.1	4.60	4.66	4.89	6.25	6.37	6.50	7.04	7.02	7.12
	0.2	0	5.21	5.40	5.81	7.06	7.18	7.37	7.90	7.92	8.16
		0.1	5.25	5.39	5.71	7.00	7.06	7.24	7.81	7.85	7.97
		0.2	5.14	5.36	5.76	6.91	7.01	7.23	7.69	7.76	8.00
	0.3	0	6.40	6.59	7.08	8.30	8.36	8.51	9.23	9.30	9.34
		0.15	5.99	6.33	6.62	7.83	7.97	8.19	8.72	8.76	8.81
		0.3	5.88	6.12	6.42	7.63	7.78	7.82	8.48	8.40	8.51
3	0	0	3.99	3.99	3.99	5.61	5.61	5.61	6.30	6.30	6.30
	0.1	0	4.60	4.72	4.89	6.53	6.60	6.65	7.37	7.42	7.55
		0.05	4.68	4.80	5.02	6.54	6.59	6.67	7.35	7.38	7.54
		0.1	4.76	4.87	4.99	6.54	6.58	6.69	7.32	7.39	7.46
	0.2	0	5.64	5.85	6.08	7.81	7.95	8.05	8.93	9.00	9.04
		0.1	5.58	5.74	5.95	7.61	7.68	7.89	8.68	8.69	8.75
		0.2	5.50	5.70	6.04	7.47	7.62	7.75	8.44	8.51	8.55
	0.3	0	7.19	7.40	7.13	9.10	8.95	9.07	10.15	10.10	9.59
		0.15	6.67	6.85	7.65	9.68	9.80	8.63	9.54	9.53	10.04
		0.3	6.45	6.51	6.86	8.50	8.57	9.70	11.14	11.03	10.75

Table 3.13 The percentage improvement of F_s during the increment of ϕ from 35° to 45°

λ	k_h	k_v	α_1=0.2			α_1=0.5			α_1=0.8		
			β=25°	β=45°	β=65°	β=25°	β=45°	β=65°	β=25°	β=45°	β=65°
0	0	0	8.23	8.23	8.23	11.63	11.63	11.63	13.03	13.03	13.03
	0.1	0	8.95	9.34	9.55	12.14	12.39	12.64	13.58	13.71	13.92
		0.05	12.02	9.38	9.85	13.26	12.33	12.77	14.29	13.75	14.11
		0.1	10.19	9.38	9.81	12.34	13.38	12.86	14.39	14.59	14.05
	0.2	0	9.32	10.48	11.11	14.25	12.73	13.73	14.71	13.95	14.81
		0.1	10.23	10.41	11.23	12.28	13.37	14.05	13.70	14.52	14.97
		0.2	11.90	10.96	10.90	13.17	14.71	14.04	14.18	15.71	15.09
	0.3	0	10.22	11.74	13.11	14.12	13.53	15.59	15.22	14.59	16.30
		0.15	11.43	11.62	12.66	13.18	14.51	14.94	14.57	15.37	15.95
		0.3	11.19	11.52	12.72	13.85	14.25	14.92	15.01	15.37	15.83
1.5	0	0	8.33	8.33	8.33	11.59	11.59	11.59	13.11	13.11	13.11
	0.1	0	9.35	9.53	9.85	12.80	12.93	13.33	14.35	14.47	14.75
		0.05	9.47	9.73	10.15	12.84	13.02	13.27	14.46	14.54	14.77
		0.1	10.13	9.68	10.17	13.22	13.11	13.40	14.46	14.60	14.75
	0.2	0	10.19	11.31	11.92	14.30	14.75	15.20	16.28	16.44	16.79
		0.1	10.87	11.17	11.88	14.38	14.62	14.94	16.03	16.23	16.44
		0.2	11.44	11.28	11.84	14.53	14.56	14.93	15.90	15.98	16.40
	0.3	0	12.53	13.62	14.51	16.91	17.29	17.55	19.09	19.10	19.25
		0.15	12.52	12.95	13.60	16.19	16.40	16.78	18.00	18.01	18.19
		0.3	12.34	12.72	13.21	15.71	15.91	16.32	17.35	17.42	17.60
3	0	0	8.36	8.36	8.36	11.63	11.63	11.63	13.03	13.03	13.03
	0.1	0	9.61	9.80	10.24	13.45	13.60	13.85	15.22	15.34	15.52
		0.05	9.79	9.96	10.37	13.48	13.60	13.85	15.20	15.28	15.51
		0.1	9.89	10.04	10.39	13.49	13.64	13.84	15.16	15.26	15.42
	0.2	0	11.65	12.04	12.63	16.06	16.30	16.55	18.42	18.48	18.55
		0.1	11.47	11.82	12.39	15.67	15.90	16.25	17.87	17.91	18.04
		0.2	11.51	11.75	12.37	15.48	15.67	15.90	17.40	17.52	17.65
	0.3	0	14.91	15.30	15.08	19.46	18.71	18.69	20.91	20.85	20.06
		0.15	13.80	14.20	15.53	19.20	20.00	18.18	20.82	19.64	20.24
		0.3	13.19	13.55	14.08	17.46	17.55	19.59	21.74	22.72	22.25

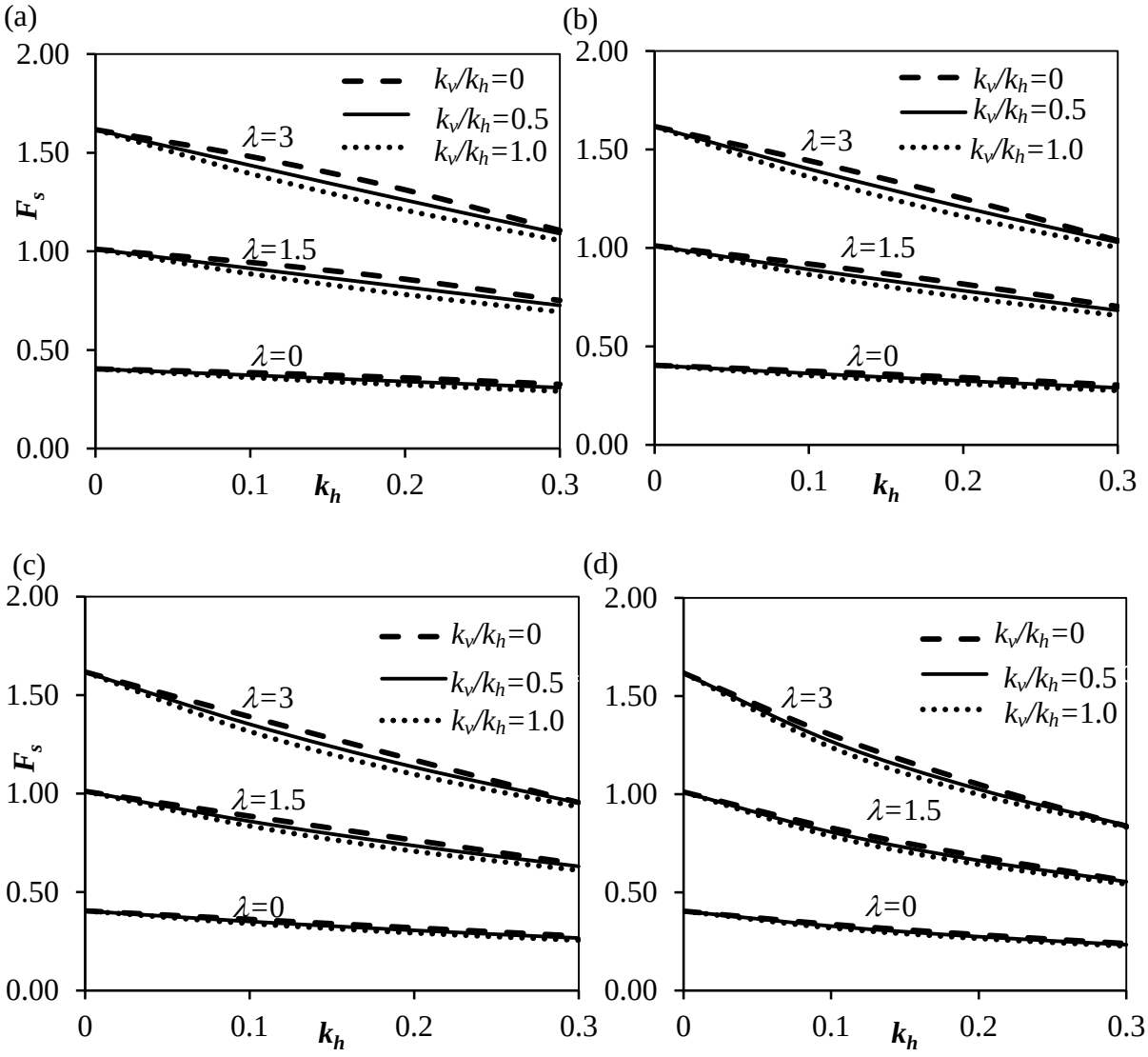

Fig. 3.12 Variation of critical factor of safety (F_s) with k_h for: (a) β=20º; (b) β=30º; (c) β=40º; (d) β=50º corresponding to α_1=0.2.

Fig. 3.14 illustrates the shape of the critical slip surface for β=20^o, 40^o, 60^o, and 80^o with a different combination of k_h. The magnitude of λ and k_v are kept as 3 and 0, respectively. The shape of the critical slip surface changes markedly with the geometric profile of the slope. The figures also give an impression that the volume of soil encompassed within the critical slip surface grown in size with the increment of the seismic forces and decrement of the slope angle.

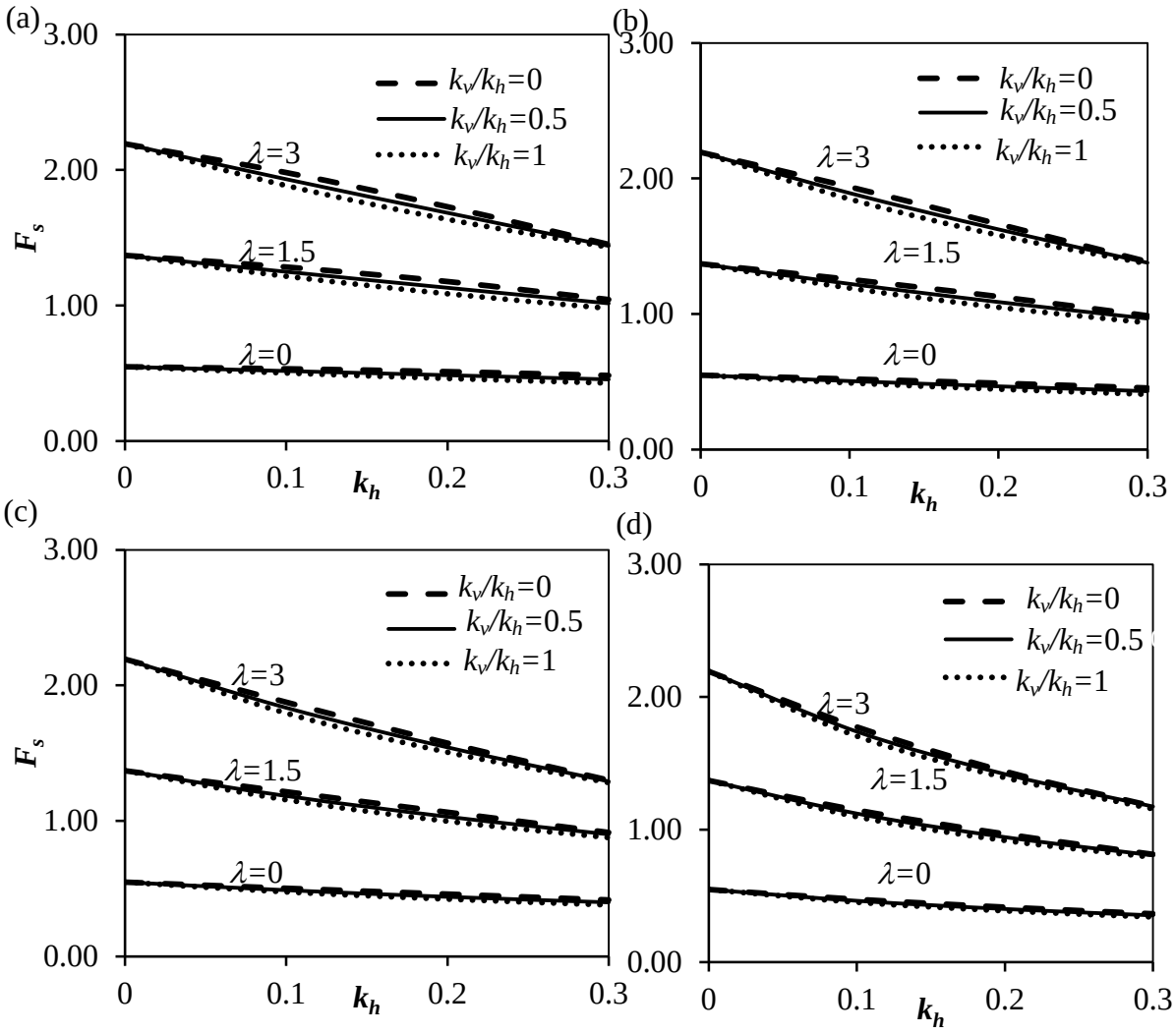

Fig 3.13 Variation of critical factor of safety (F_s) with k_h for: (a) β=20º; (b) β=30º; (c) β=40º; (d) β=50º corresponding to α_1=0.6.

3.5 VERIFICATIONS WITH EXISTING LITERATURES

The computational results for four cases obtained from the analysis, in Section 3.5, have been compared with the available literature and these comparisons have been presented accordingly in this particular section.

3.5.1. Case 1: Homogeneous c-ϕ soil

Table 3.14 shows the comparison of the present obtained solutions from the variational approach with the results provided by Newmark (1965) and Choudhury et

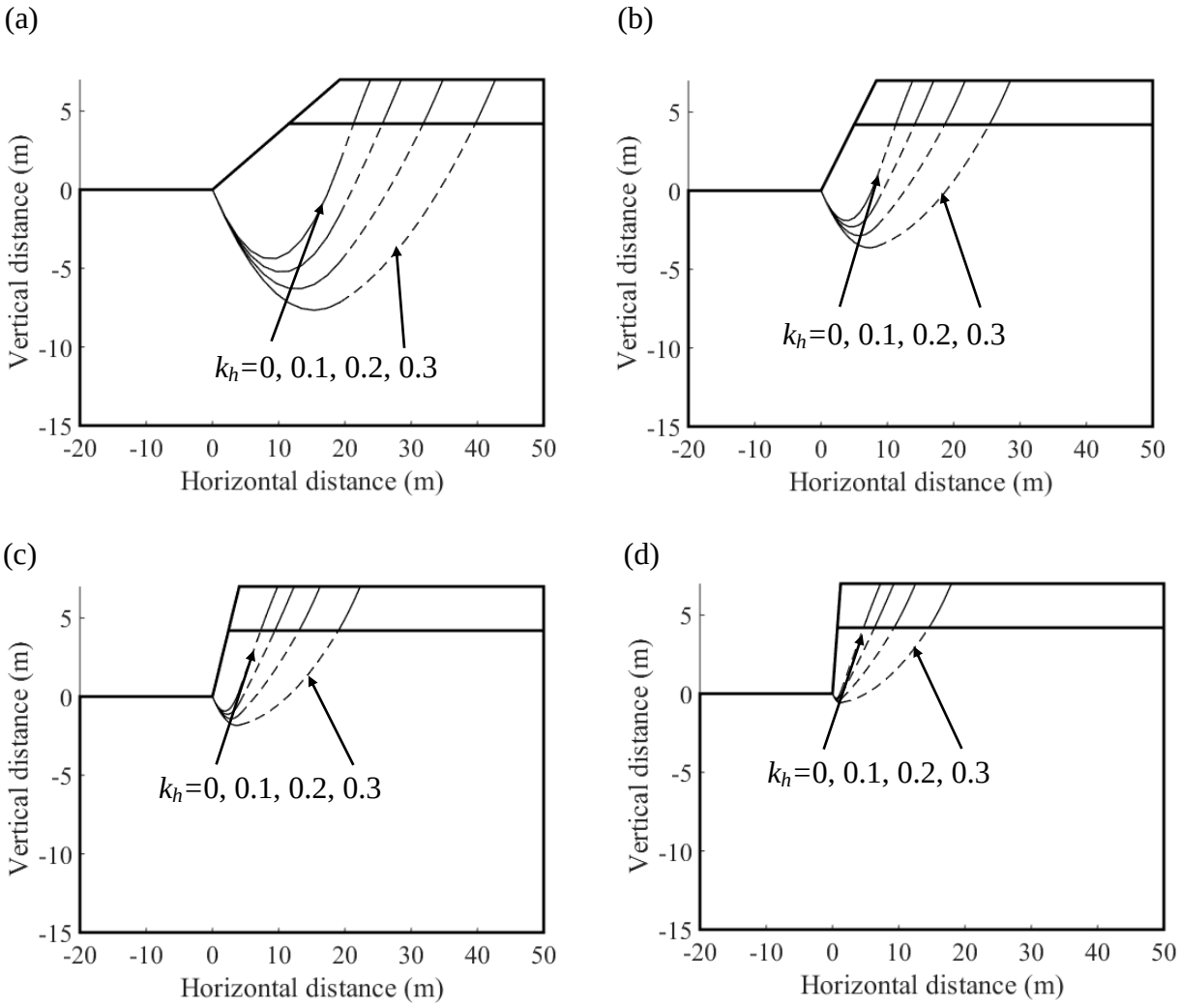

Fig 3.14 Form of the critical slip surfaces for: (a) β=20^o, λ=3, α_1=0.4, k_v=0; (b) β=40^o, λ=3, α_1=0.4, k_v=0; (c) β=60^o, λ=3, α_1=0.4, k_v=0 (d) β=80^o, λ=3, α_1=0.4, k_v=0.

al. (2007). The comparisons are carried out for different values of ϕ and k_h correspond to three different β, namely, 20^0, 25^0, and, 30^0. In this comparative study, the magnitude of k_v is kept equal to zero. The present analytical solutions are quite agreeable with the available solutions. It is to be noted that Newmark (1965) assumed the failure surface to be planar and Choudhury et al. (2007) considered the failure surface to be circular. However, in the present study there was no such approximation prior to the analysis.

Table 3.14 A comparison of F_s values obtained by Newmark (1965) and Choudhury et al. (2007) with the present solutions considering k_v=0

		β=20^0			β=25^0			β=30^0		
ϕ	k_h	Newmark (1965)	Choudhury et al. (2007)	Present study	Newmark (1965)	Choudhury et al. (2007)	Present study	Newmark (1965)	Choudhury et al. (2007)	Present study
35^0	0.1	1.45	1.31	1.57	1.37	1.25	1.30	-	-	1.11
	0.2	1.15	1.15	1.26	-	-	1.08	-	-	0.93
40^0	0.1	1.74	1.35	1.86	1.72	1.34	1.54	1.48	1.19	1.31
	0.2	1.38	1.2	1.50	1.34	1.1	1.27	-	-	1.09
	0.3	1.13	1.04	1.25	-	-	1.08	-	-	0.94
45^0	0.1	2.08	1.63	2.20	2.01	1.61	1.81	1.79	1.43	1.53
	0.2	1.64	1.44	1.77	1.62	1.43	1.49	1.52	1.30	1.28
	0.3	1.34	1.28	1.48	1.31	1.21	1.27	-	-	1.10

3.5.2 Case 2: Non-homogeneous undrained cohesive soil (ϕ_u=0°)

Table 3.15 shows the comparison of the present solution evaluated from the variational method with the available solution provided by Koppula (1984) and Li et al. (2018) for the static case. The comparison is carried out for different values of cohesion coefficient (λ) corresponding to various β for both static and pseudostatic case. The

Table 3.15 A comparison of F_s values obtained from the present study with the solution of Koppula (1984) and Li et al. (2018) considering k_h= k_v=0 for β = 45^o

λ	Present study	Koppula (1984)	Li et al. (2018)
0.5	0.75	1.00	1.00
1	1.00	1.27	1.27
2	1.50	1.79	1.79
3	2.00	2.31	2.31
4	2.50	2.83	2.83
5	3.00	3.34	3.34
10	5.50	5.92	5.92

present solution is compared with the available solution for a particular slope consisting of non-homogeneous purely cohesive soil with slope height, h=10m, γ = 16 kN/m^3, and c_{u0}= 20 kPa.

Table 3.16 depicts the comparison between the present solution and the result presented by Li et al. (2018) for the pseudostatic case. Koppula (1984) employed the conventional limit equilibrium method (LEM) where the shape of the slip surface was pre-assumed as circular. Conversely, Li et al. (2018) applied variational method based

Table 3.16 A comparison of F_s values obtained from the present study with the solution of Li et al. (2018) considering k_v=0

		β=60^o		β=75^o	
k_h	λ	Present study	Li et al. (2018)	Present study	Li et al. (2018)
0.1	0	0.44	0.57	0.43	0.50
	0.5	0.66	0.74	0.64	0.66
	1	0.88	0.96	0.85	0.78
	1.5	1.10	1.14	1.06	0.89
	2	1.31	1.25	1.28	1.04
	2.5	1.53	1.39	1.49	1.25
	3	1.75	1.79	1.70	1.39
0.2	0	0.38	0.54	0.36	0.45
	0.5	0.57	0.66	0.54	0.57
	1	0.76	0.83	0.72	0.69
	1.5	0.95	0.96	0.90	0.83
	2	1.14	1.14	1.08	0.96
	2.5	1.33	1.25	1.26	1.04
	3	1.52	1.39	1.43	1.25

on LEM, assuming a circular slip surface in the case of ϕ=0. In contrast, the present analysis does not necessitate such prior assumption regarding the shape of the slip surface. Moreover, the present computed slip surfaces seem to encompass larger soil mass; this eventually indicates larger driving force and, hence, leads to a lower

estimation of F_s. Consequently, the magnitude of F_s prescribed by Koppula (1984) and Li et al. (2018) are identical and the estimated F_s values from the present study are smaller than the solutions obtained from Koppula (1984) and Li et al. (2018). The present analytical solutions are quite agreeable with the available solutions.

3.5.3 Case 3: Two layered cohesive-frictional soil

Table 3.17 shows the comparison of the present solutions obtained from the variational approach with the results provided by Kumar and Samui (2006). The comparisons are carried out for different values of ϕ_1 and ϕ_2 corresponding to three different β, namely, 45°, 65°, and, 75°. In this comparative study, the magnitude of k_v is

Table 3.17 The comparison of stability number obtained by Kumar and Samui (2006) with the present solutions considering k_v=0 and c_1/c_2=1

ϕ_1	ϕ_2	β=45°		β=65°		β=75°	
(°)	(°)	Present study	Kumar and Samui (2006)	Present study	Kumar and Samui (2006)	Present study	Kumar and Samui (2006)
10	20	0.077 (0.091)	0.072 (0.100)	0.104 (0.120)	0.111 (0.133)	0.118 (0.136)	0.125 (0.154)
	30	0.058 (0.069)	0.056 (0.083)	0.084 (0.099)	0.080 (0.125)	0.099 (0.118)	0.091 (0.143)
	40	0.044 (0.066)	0.024 (0.071)	0.069 (0.092)	0.045 (0.100)	0.084 (0.107)	0.067 (0.128)
20	30	0.057 (0.060)	0.043 (0.059)	0.081 (0.090)	0.067 (0.091)	0.094 (0.102)	0.111 (0.125)
	40	0.044 (0.052)	0.015 (0.048)	0.067 (0.078)	0.033 (0.077)	0.081 (0.095)	0.050 (0.111)
30	40	0.043 (0.051)	0.013 (0.036)	0.065 (0.075)	0.027 (0.071)	0.078 (0.091)	0.045 (0.100)

Note: The values in the parenthesis are for k_h=0.1

kept equal to zero and the value of k_h is taken to be 0 and 0.1. The present analytical solutions are quite agreeable with the available solutions. It is to be noted that Kumar and Samui (2006) assumed the shape of the failure surface as log-spiral. However, in

the present study, the shape of failure surface is obtained as parabolic in different segments as expressed in Eq. (3.15). The expression of N as considered in the work of Kumar and Samui (2006) is reciprocal to the present definition and hence, the numerical solutions reported in their work are inverted and compared thereafter.

3.5.4 Case 4: Homogeneous c-ϕ soil underlain by non-homogeneous clays

The comparison is carried out for various magnitudes of cohesion coefficient (λ) corresponding to different β for both static and pseudostatic case. Table 3.18 illustrates the comparative study between the present solution and the obtainable result provided by Hunter and Schuster (1968), Griffiths and Yu (2015) and Hossley and Leshchinsky (2019) for Static case (k_h= k_v=0). Hunter and Schuster (1968) applied ϕ=0 limit equilibrium method to solve the non-homogeneous slope with linearly varying cohesion problem considering circular slip surface. Hunter and Schuster (1968) considered the cohesion of soil at the ground surface (c_{u0}) greater than zero. Griffiths and Yu (2015) implemented Matlab optimization programs to assess the location of critical slip circle and evaluate corresponding critical factor of safety of linearly increasing undrained cohesive slopes. Hossley and Leshchinsky (2019) employed lower bound finite element limit analysis and studied the influence on slope stability for various slope geometry, slope of soil profile and inclination of c_u profile. These three researchers presented the results in terms of stability number (N) but in the present analysis, the solutions are provided as factor of safety (F_s). To enhance comprehension of the comparison, the stability number solutions presented by Hunter and Schuster (1968), Griffiths and Yu (2015), and Hossley and Leshchinsky (2019) are converted into a factor of safety. This conversion is accomplished by employing the mathematical relationship between the

stability number and factor of safety, as outlined in their respective research articles ($N_s = F_s\gamma/m$).The comparison is carried out for the slope of height, h=10m by taking into account material parameters, γ = 20 kN/m^3, c_{u0}= 20 kPa and m= 1 kN/m^3. As comparing the present solution with the available result presented by Hunter and Schuster (1968), Griffiths and Yu (2015) and Hossley and Leshchinsky (2019), a similar increasing trend of F_s is observed

Table 3.18 A comparison of F_s values obtained from the present study with the solution of Hunter and Schuster (1968), Griffiths and Yu (2015) and Hossley and Leshchinsky (2019) considering $k_h = k_v$=0

β (o)	λ	Present Study	Hunter and Schuster (1968)	Griffiths and Yu (2015)	Hossley and Leshchinsky (2019)
30	0.5	0.60	0.47	0.46	0.44
	1.0	0.80	0.61	0.61	0.60
	2.0	1.20	0.94	0.93	0.92
40	0.5	0.60	0.41	0.39	0.38
	1.0	0.80	0.55	0.55	0.54
	2.0	1.20	0.86	0.85	0.84
50	0.5	0.60	0.35	0.34	0.34
	1.0	0.80	0.48	0.48	0.47
	2.0	1.20	0.77	0.76	0.75
60	0.5	0.60	0.31	0.30	0.30
	1.0	0.80	0.42	0.42	0.42
	2.0	1.20	0.70	0.69	0.68
70	0.5	0.60	0.28	0.28	0.27
	1.0	0.80	0.34	0.34	0.35
	2.0	1.20	0.62	0.61	0.61
80	0.5	0.60	0.24	0.24	0.23
	1.0	0.80	0.33	0.33	0.34
	2.0	1.20	0.56	0.56	0.55
90	0.5	0.60	0.22	0.22	0.21
	1.0	0.80	0.29	0.29	0.30
	2.0	1.20	0.49	0.49	0.48

when λ changes. Table 3.16 depicts the comparison between the present solution and the result presented by Li et al. (2018) for the pseudostatic case. Although Li et al.

(2018) applied variational method to analyze soil slopes but the formulations are quite different from the present analysis. The present analytical solutions are quite agreeable with the available solutions.

3.6 SUMMARY

The present chapter focuses on the development of the variational method to account the effect of heterogeneity, seismicity, and frictional strength. Based on D'alembert's principle, the pseudo-static approach is adopted to model the effects of seismic loading. The solution of variational method appears to be more realistic than the conventional LEM solutions as there is no need of incorporating any static and kinematical assumptions. By performing functional optimization, the critical slip surfaces and the corresponding critical factor of safety are attained. Based on the configuration of soil profiles four different cases are dealt with: (i) homogeneous c-ϕ soil, (ii) non-homogeneous undrained cohesive soil (ϕ_u=0°), (iii) two layered cohesive-frictional soil, and (iv) homogeneous c-ϕ soil underlain by non-homogeneous clays. For each case, the design charts are prepared to showcase the effects of various material properties, geometrical configurations, seismic loadings on the critical factor of safety. It is observed that the factor of safety decreases with an increase in seismic forces and a decrease in soil strength. The increase in slope angle appears to be more detrimental for the slopes experiencing pseudo-static loading. The critical slip surfaces are plotted for several cases, and the obtained solutions are compared with existing solutions, validating the accuracy and reliability of the variational method used. Overall, the provided design charts and analytical formulations offer practical tools for assessing the stability of slopes in different scenarios, be it homogeneous or non-homogeneous soil slopes subjected to seismic forces.

3.7 LIMITATIONS

As the variational method is primarily developed on the principles of LEM, therefore few shortcomings such as, ignoring stress-strain and strain-displacement relationships, incapability of tackling complicated geometries, arbitrary boundary conditions, complex loading conditions, and random soil properties, associated with the LEM, are also retained over here. Hence, the present solutions are not rigorous and cannot be guaranteed as either of the extremities (upper/lower bound) on the true collapse load. The proposed formulations are based solely on the strength parameters; therefore, the computed F_s values are insensitive to the stiffness parameters. Moreover, the proposed stability charts are applicable within specific parameter ranges; in cases where the required field falls outside these ranges, determining the critical factor of safety can be readily achieved through the provided formulations. However, the novelty of the present work is to propose new formulation for estimating the safety factor of different pseudostatic soil slopes using the calculus of variation.